SOLAR PHOTOCATALYTIC DEGRADATION OF ORGANIC POLLUTANTS IN LOCAL DYEING WASTEWATER USING NEEM-MODIFIED GRAPHITIC CARBON NITRIDE (g-C_3N_4)

The discharge of dyeing wastewater containing high concentration of contaminants from the local dyeing industry has caused a serious environmental concern. The present study reports the synthesis of graphitic carbon nitride and itsutilization in degradation of dyeing effluent pollutants under solar irradiation. The synthesized g-C_3N_4 was modified using the aqueous leaves extract of AzadiratchaIndica (Neem plant): a clean, non-hazardous and environmentally friendly procedure (green modification route). The morphology, elemental composition, crystallography, Surface area and adsorption bands of the synthesized modified and unmodified g-C_3N_4 samples were comprehensively examined using SEM, EDS, XRD, FT-IR and BET characterization techniques. The photo-oxidation of organic pollutants in the local dyeing wastewater by the modified and unmodified g-C_3N_4nanomaterials under sunlight irradiation in a batch reactor system was tested. The photocatalytic degradation efficiency of the local dyeing wastewater by the photocatalysts was assessed using chemical oxygen demand (COD) as the indicator parameter. Different experimental conditions such as the effects of solution pH, time, and Photocatalyst dosage on the efficiency of COD degradation process were investigated and then optimum conditions were established. The SEM and XRD analysis of the modified and unmodified g-C_3N_4demontrated the formation of crystalline tri-s-triazine unit and agglomerated morphology. The BET surface analysis displayed that the surface area of the g-C_3N_4nanopaticles increased from 58.88 cm^3/g to 141.0 cm^3/g upon modification, while the EDS analysis demonstrated the existence of C and N as the major constituents of the as-synthesized nanomaterials. The study found that the modified g-C_3N_4 nanoparticle exhibited significant higher catalytic activity of 61% COD removal compared to the unmodified g-C_3N_4nanoprticle (40% COD removal). It was established from the optimization study that pH of 9.8 and photocatalyst dosage of 0.7 g/200ml were the optimum conditions. The experimental data obtained were evaluated

using three different kinetic models: first order, second order and Behnajady-Modirshahla-Ghanbery (BMG). It was found that the Behnajady-Modirshahla-Ghanbery model best described the data based on the correlation coefficient (R^2). This study demonstrated that the modified g-C_3N_4 nanoparticle showed better photocatalytic activity in comparison to the unmodified g-C_3N_4. The enhancement in performance is because of its high surface area which signifies more active sites for reaction, small bulk diffusion length and strong redox ability of charge carriers.

CHAPTER ONE

1.0 INTRODUCTION

1.1 Background to the Study

Water is life and remains an essential resource required for human survival, socio-economic and political stability (Cantrella *et al*., 2015). However, 0.01% out of 0.7% total available water is only available for human consumption (Gupta *et al*., 2015). Today, the most discussed issues around the globe by both government and non-governmental organizations at different forums are sanitation, land, air and water pollution (Khalid *et al*., 2017). The quality and quantity of water has continued to deteriorate due to natural and anthropogenic activities such as flooding, rapid population increase, poor agricultural practices, industrial expansion and climate change coupled with urbanization (Das, 2014). Specifically, human activities are responsible for huge generation and disposal of toxic wastes into the environment, with a consequential impact on surface and groundwater quality (Gupta *et al*., 2013). Almost all of the natural sources of drinking water such as surface water, groundwater, lakes and reservoirs, rivers and canals, and rainwater have been reported to be contaminated with toxic materials and pathogenic microorganisms (Baruah *et al*., 2015). For instance, the dyeing industries in Nigeria use and dispose complex organic dyes and inorganic constituents which are toxic, persistent and non-biodegradable into the water ways, thereby causing devastating effects on both human and aquatic life (Lee *et al*., 2016). The local dyeing industry utilizes large amount of water and at the same time generate large volume of wastewater containing complex organic dyes, thus require proper treatment prior to discharge into the environment (Ghaly, *et al*., 2014). These organic dyes at low and high concentrations are considered as environmental nuisance and continuous exposure to such wastewater can cause disruption of endocrine glands and respiratory system

depending on the exposure time and dosage (Hadi and Wahab, 2015). The organic dyes in the dyeing waste water are responsible for the intense coloration notice in Rivers which inhibits sunlight, increase the level of chemical oxygen demand (COD), biological oxygen demand (BOD), and also obstruct photosynthesis and reoxygenation processes (Ghaly *et al*., 2014). Other chemicals in the wastewaters include dispersants, leveling agents, acids, alkalis, carriers and various dyes and the pH of water bodies (Gupta and Suhas. 2013). With an increase in the use of different varieties of dyes, pollution by dye wastewater is becoming increasingly alarming and thus become imperative to treat such wastewater prior to discharge in order to reduce associated risks in the environment (Das, 2014).

Several conventional wastewater treatment methods such as flocculation (Ghaly *et al*., 2014), coagulation (Sadi *et al*., 2015) ozonation (Khaki *et al*., 2017), biological treatments (Hu, 2013), adsorption (Harikumar *et al*., 2013), electrodialysis (Baruah *et al*., 2015), reverse osmosis (Dariani *et al*., 2016), ion exchange (Ghaly *et al*., 2014), precipitation (Ying, 2015) among others have been applied to treat local dyeing wastewater. However, these methods have certain shortcomings such as high cost of chemical/ reagents, complex treatment procedure, generation of toxic sludge, low efficiency as regards degradation of organic pollutants (Hu, 2013).

Recently, advanced oxidation processes (AOPs) involving photocatalysis has been identified as an efficient technique for the decomposition of organic dyes in local dyeing wastewaters into harmless substances such as CO_2 and H_2O based on radical mechanism (Sarnali and Bhagchandani, 2016). More so, semi-conductor metal oxides and non metals such as vanadium, chromium, titanium, zinc , tin and carbon nitride exhibit excellent photocatalytic activity in the presence of light source and induce a charge separation process with the formation of positive holes which oxidize organic substrates (Hisatomi *et al*., 2014). In this process, a photocatalyst is

activated with either UV light, visible light or a combination of both, and photo exited electrons are elevated from the valence band to the conduction band, forming an electron/hole pair (e^-/h^+) (Khaki *et al*., 2017). The photo generated pair (e^-/h^+) is able to reduce and /or oxidize a compound absorbed on the photocatalyst surface (Das, 2014). Among the non metal photocatalysts, graphitic carbon nitride (g-C_3N_4) nanoparticles is considered due to its exceptional features such as non-toxicity, stable chemical properties, mild band gap (2.7 eV), absorption of visible light (Niu *et al*., 2012). Despite these unique features, graphitic carbon nitride still has limitations for practical applications due to low efficiency of visible light utilization, high recombination rate of the photo generated charge carriers, low electrical conductivity and small specific surface area (<10 m^2g^{-1}) (Niu *et al*., 2012). Furthermore, researchers have employed different strategies to solve problems associated with g-C_3N_4 based photocatalyst, which is through modification. This modification strategy involves the incorporation of foreign impurities such as metals (Ag, Pd, Pt, and Au) and non metals (C, S, F, and N) into the crystal lattice layer of g-C_3N_4 nanoparticles (Khaki *et al*., 2017). These foreign impurities mostly serve as electron trappers and prevent high electron-hole recombination rate.

Green synthesis involving the use of plant extracts or microorganisms as reducing agents has been identified as an alternative route to prepare nanoparticles of desired shapes and sizes due to its relative abundance, cost effectiveness and environmental friendliness (Deepa *et al*., 2016). In this study, g-C_3N_4 nanoparticles will be synthesized and then modified with the leaf extract of Azadirachta Indica (Neem).The neem leaf extract, when integrated into the crystal lattice of g-C_3N_4 nanoparticles, will create a synergy thereby reducing the band gap energy and enhancing the surface area. In addition, the photocatalytic activity of the prepared g-C_3N_4 nanoparticles under sunlight using local dyeing wastewater will be investigated.

1.2 Statement of the Research Problem

Environmental pollution and inadequate disposal of local dyeing wastewater containing organic dyes have become an increasing menace in Nigeria. Exposure to low or high amounts of organic dyes in such wastewater causes detrimental effects on human and aquatic life. There is also the challenge of discoloration factor from dyes when expelled into land or into water bodies which eventually distorts the ecosystem. Similarly, local dyeing wastewaters have offensive odour and continuous exposure can cause skin hemorrhage and lesions (Nese *et al*., 2007).

Current conventional wastewater treatment methods such as flocculation, ion exchange, coagulation, distillation, filtration, reverse osmosis and adsorption are not suitable for the eradication of toxic organic dyes (Pokharna and Shivastava, 2013). In addition, adsorption technology produces toxic sludge, and transforms pollutants from one phase to another (Maletz *et al*., 2013).

Despite graphitic carbon nitride having some advantages such as mild band gap (2.7 eV), absorption of visible light and flexibility, it still has limitations for practical applications due to low efficiency of visible light utilization, high recombination rate of the photo generated charge carriers, low electrical conductivity and small specific surface area (<10 m^2g^{-1}) (Niu *et al*., 2012). Thus, modification of the photocatalysts with the aim of ensuring high efficiency, fast separation of electron/hole pair and increased surface area is required.

1.3 Justification of the Research

Photocatalysis is identified as a logical technique to treat local dyeing wastewater and achieve mineralization of toxic organic dyes molecules into CO_2 and H_2O compared to other conventional methods (Baruah *et al*., 2015). Synthesis and modification of g-C_3N_4 via green

route, where the plant extract is used as a reducing/capping and stabilizing agent will help to solve the problem of contamination and formation of hazardous bye products. This method is relatively cheap, eco-friendly, and highly efficient method due to non usage of toxic precursors as compared to other chemical and physical synthesis methods. Modification of the g-C_3N_4 with the neem leaf extract solution helps to increase the surface area, suppress electron/hole recombination and subsequently enhance the photocatalytic efficiency of the g-C_3N_4 nanoparticle.

1.4 Aim and Objectives of the Study

The aim of this work is to study the solar photocatalytic degradation of organic pollutants in local dyeing wastewater using neem-modified graphitic-carbon nitride (g-C_3N_4) photocatalyst.

The aim of this study is to be achieved through the following objectives;

i. Synthesis of g-C_3N_4 nanoparticles using melamine as the precursor.
ii. Modification of the as-synthesized g-C_3N_4 using nem leaf extract
iii. Characterization of the modified g-C_3N_4 photocatalyst
iv. Evaluations of the phytochemicals present in the neem leaf extract solution.
v. Performance evaluation of the modified g-C_3N_4 using chemical oxygen demand (COD) reduction as the response, with respect to the effects of time, solution pH and catalyst dosage.
vi. Evaluate the kinetics of the photocatalytic reaction process.

1.5 Scope of the Study

The scope of this research work is limited to the synthesis of graphitic-carbon nitride (g-C_3N_4) photocatalyst, modification of the as-synthesized photocatalyst and its application in the degradation of organic pollutants in local dyeing wastewater.

CHAPTER TWO

2.0 LITERATURE REVIEW

2.1 Methodology for Wastewater Treatment

Several methods which have been applied for the wastewater treatments can be generally classified in three categories (i) chemical (ii) physical (iii) biological (Robinson *et al*., 2001). The comprehensive branching and sub-divisions has been schematically shown in Figure 2.1.

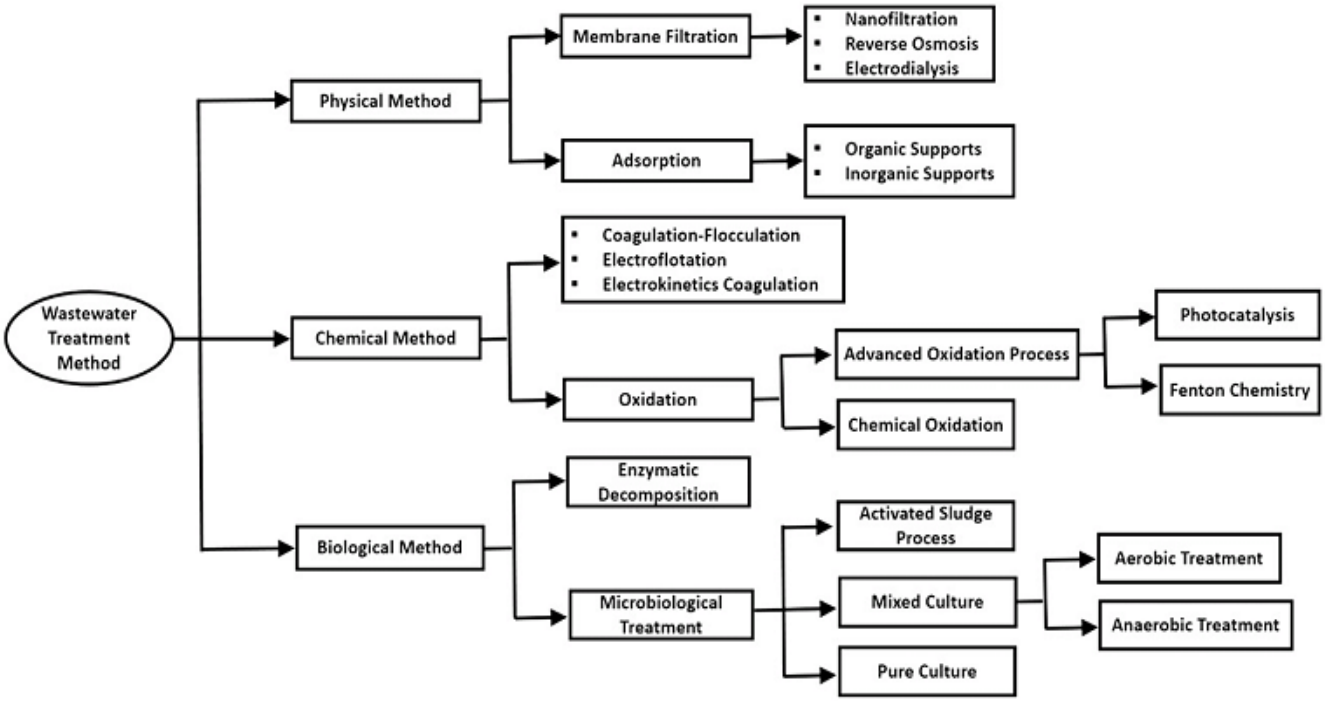

Figure 2.1: Wastewater Treatment Methodologies (Robinson *et al*., 2001)

2.1.1 Chemical Process: Chemical route is a system that uses reagents to convert, reduce, or oxidize organic compounds in wastewater into nontoxic components. These methods comprise coagulation or flocculation techniques combined with flotation and filtration, electrokinetic

coagulation electroflotation, oxidation methods (Holkar *et al*., 2016). This is frequently considered as one of the robust ways of eliminating color from the wastewater. Among all chemical processes, oxidation technique is the most regularly used chemical decoloration practice owing to its easy of appliance. This technique is further categorized into chemical oxidation and advance oxidation process (AOP). These methods have the capability to break down chemical dyes and pesticides totally under ambient conditions (Holkar *et al*., 2016). These AOP process can further be identified as photocatalytic oxidation (use of light for activation of catalyst) and fenton chemistry appropriate for treating wastewater which are challenging to biological treatment (Holkar *et al*., 2016).

2.1.2 Physical Process: Physical methods commonly used for wastewater treatments consist of membrane-filtration processes (nanofiltration, electrodialysis, reverse osmosis) and adsorption practice (Holkar *et al*., 2016). The main drawback of the membrane technologies is that they have a finite lifetime before membrane fouling occurs and the cost incurred during intermittent replacement must as a consequence, be integrated in any breakdown of their economic feasibility. Adsorption technique provides an alternative approach and is better and effective than any other physical method particularly if the sorbent is cheap and does not involve further pre-treatment step before its application. Activated carbon is the most effective adsorbent for a broad range of dyes. However, the regeneration process or the transfer of pollutants from one medium to another is detrimental to the environment (Robinson *et al*., 2001).

2.1.3 Biological Process: It is commonly considered as the most inexpensive technique used for wastewater treatment in comparison with the chemical and physical methods. Several microorganisms like, bacteria, yeasts, algae and fungi are able to degrade different pollutants and hence, used for the treatment of industrial effluents (Satyawali and Balakrishnan, 2008). Based

on the mode of operation, biological method can be classified into aerobic, anaerobic, anoxic, facultative or a combination of these. Their application is often restricted as a consequence of technical constraints. Large land area is one of the most important requirements of Biological treatment and is limited by sensitivity toward diurnal variation as well as poisonous effect of some chemicals and constrained flexibility in design and function (Bhattacharyya and Sarma, 2003). Biological treatment lacks the ability to obtain satisfactory color removal with the present conventional biodegradation practices. Moreover, while various organic pollutants are degraded, several others are difficult to be removed as a consequence of their complicated chemical composition and organic nature (Robinson *et al*., 2001).

The present wastewater treatment practices such as adsorption, electrochemical oxidation, coagulation do not totally get rid of the pollutants contained in the wastewater and thus, lead to generation of a more concentrated pollutant-containing phase (Padmanabhan *et al*., 2006). Other water treatment methods such as sedimentation, filtration, chemical and membrane technologies have high operating costs and involve the possible risk of producing harmful secondary pollutants into the environment (Gaya and Abdullah, 2008). Chlorination has been the most popular and widely adopted disinfection process. The disinfection by-products that emanate from chlorination are mutagenic and carcinogenic to human health (Yang and Cheng, 2007). These have consequently resulted to the increase in research and development in the field of advanced oxidation process to improve in oxidative reduction of the organic compounds dissipated or dissolved in the wastewater. Among them heterogeneous photocatalysis is attracting researchers' attention due to its high effectiveness in degrading all the organic pollutants present in the wastewater (Blake, 2001).

2.2 Photocatalysis

Photocatalysis is a significant AOP technique for decomposition of organic compounds with a high total organic carbon (TOC) removal at mild operating conditions of temperature and pressure. This technique is relied on the additive catalyst into the wastewater with illumination of UV radiation, which can degrade organic pollutants to carbon dioxide and water by an effective and eco-friendly way. In addition, this technique can be operated at neutral pH and does not form by-product of complex sediment. An efficient photocatalyst is defined as a concordantly combination of chemical and photoelectronic properties, as a result of activations of a semiconductor material. Various types of semiconductor materials, such as TiO_2, ZnO, ZnS, g-C_3N_4 have been developed for photocatalytic oxidation of organic contaminants in the remediation of wastewater (Liqiang, 2004). Photocatalytic process is achieved with the absorption of photos by a semiconductor material thereby generating electrons that migrate from the valence band (VB) to conduction band (CB), thus, generating electron (e^-)/hole (h^+) pairs. The hole (h^+) will react with water and hydroxyl anions to produce hydroxyl radicals ($^\bullet$OH). The possible reasons which may be assigned to photocatalysis gaining high importance in wastewater treatment are as follows (Bhatkhande *et al*., 2002):

(i) Illustrating total mineralization of most of the organic pollutants

(ii) Ability to operate in ambient temperature

(iii) No disposal issues (in water)

(iv) Pathways for an economic and environmentally-friendly solution.

2.3 Fundamentals and Mechanism of Photocatalysis

Photocatalysis in general operate through the principal of band gap (and interactions involving the same), i.e., different classes of semiconductor materials cater to the need of various photocatalytic applications. Traditionally, semiconductors exhibit an empty energy region in which no energy levels are available to promote the recombination of an electron and hole produced by photoactivation in the solid which is unlike metals, i.e., having a continuum of electronic states. For a semiconductor to be photo-chemically active, the redox potential of the photogenerated conductance band electron must be sufficiently negative and photogenerated valence band must be sufficiently positive so that electron can reduce the adsorbed O_2 to superoxide and hole can generate the ●OH radicals (most potent oxidizing agents) which will then subsequently oxidize the organic pollutants (Chong *et al*., 2010). On irradiation of light (Ultraviolet or Visible) absorption of photon takes place in semiconductor materials and excites an electron (e^-) from the valence band to the conduction band if the photon energy ($h\upsilon$), equals or greater than the band gap of the semiconductor/photocatalyst. During excitation of an electron (e^-), simultaneously, a hole (h^+, positive charge) is generated in the valence band (schematically shown in Figure 2.2).

$$h\upsilon + \text{Semiconductor} \rightarrow h^+ + e^- \qquad 2.1$$

On the generation of electron-hole ($e^- - h^+$) pair, mainly two possibilities exists (i) recombination of electron and hole pair producing thermal energy in the absence of suitable scavenger or surface defect state to trap the electrons (ii) prevention of recombination and participation in redox reactions with the compound adsorbed on the photocatalyst. Although, the lifetime of an e^--h^+ pair is few nanoseconds (Bussi *et al*., 2002), it is still long enough for initiating/promoting redox reactions. Generally, the electron can be offered to an electron acceptor like a metal ion whose redox potential is more positive than the photocatalyst band gap or to an oxygen molecule

to form a superoxide radical. In the same way, a hole oxidizes water to form hydroxyl radicals (which subsequently initiate a chain of reactions leading to the oxidation of organics as shown in fig 2.2). The same can also combine with the electron from a donor species, depending on the mechanism of the photoreaction. Thus, the series of chain oxidative reductive reactions that occur at the photon activated surface can be postulated as follows (Chong *et al*., 2010):

Photoexitation**:** photocatalyst + hυ $\rightarrow h^+ + e^-$ 2.2

Charge – carrier trapping of e^-: $e^-_{CB} \rightarrow e^-_{TR}$ 2.3

Charge – carrier trapping of h^+: $h^+_{VB} \rightarrow h^+_{TR}$ 2.4

Electron – hole recombination: $e^-_{TR} + h^+_{VB}\,(h^+_{TR}) \rightarrow e^-_{CB}$ + heat 2.5

Photoexcited e^- scavenging: $(O_2)_{ads} + e^- \rightarrow O_2^{\bullet -}$ 2.6

Oxidation of hydroxyls: $OH^- + h^+ \rightarrow OH^{\bullet}$ 2.7

Photodegradation by $OH^{\bullet}$: $R - H + OH^{\bullet} \rightarrow R'^{\bullet} + H_2O$ 2.8

Here, e^-_{TR} and h^+_{TR} in Equation (2.5) represent the surface trapped conductance band electron and valence band hole respectively. For the successful functioning of photocatalysts, the recombination of electron-hole needs to be delayed. In the absence of an electron scavenger, they recombine (as shown in Equation 2.5) in nanoseconds and negatively affect the efficiency of the photocatalytic reaction. Equation (2.6) depicts prevention of recombination of electron-hole pair in the presence of oxygen and allowing the formation of superoxide radical ($O_2^{\bullet -}$) further lead to the formation of $HO^{\bullet}_2$; a radical with scavenging property (Chong *et al*., 2010).

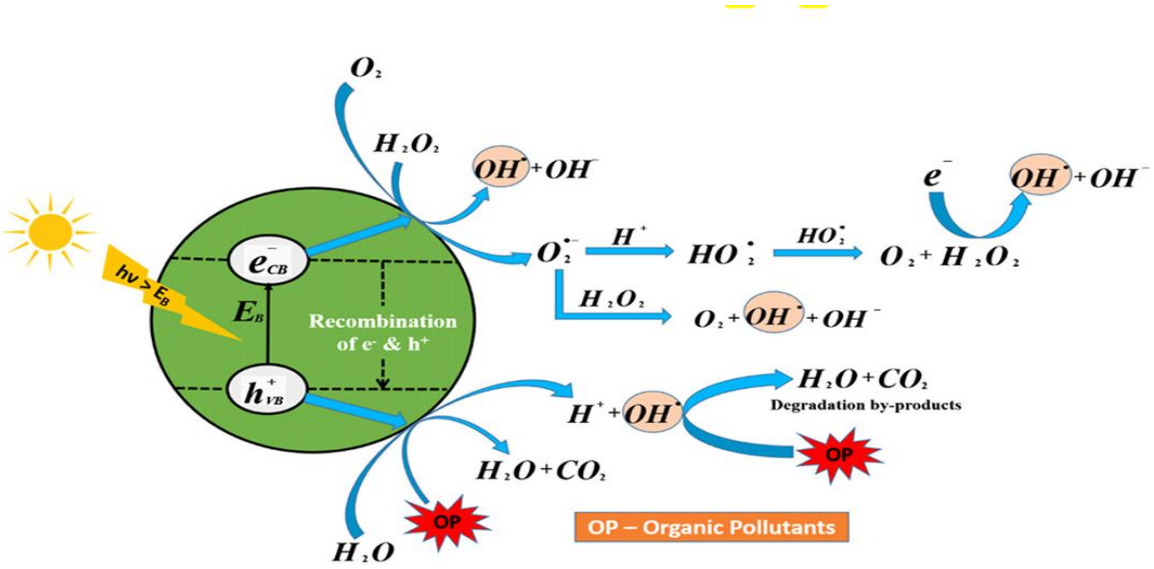

Figure 2.2: The Reaction Mechanism of Graphitic Carbon Nitride Photocatalyst

2.4 Photocatalysts

Photocatalysts are the materials which promote reaction in the presence of light and not get consumed in the overall reaction. Some of the characteristics of a good photocatalyst are (a) being photoactive (preferably visible light active) (b) chemical/biochemical inertness, (c) photostability (i.e. not liable to photo-corrosion), (d) nontoxicity (Bhatkhande *et al*., 2002).

2.5 Photocatalyst Materials

2.5.1 Metal-based Photocatalysts

The various metal based photocatalyst are discussed in detail as shown from sections 2.5.1.1 to 2.5.1.5

2.5.1.1 TiO_2 and modified TiO_2 counterparts

Titanium dioxide (TiO_2) is a typical example of semiconductor possessing three main crystalline structures which are rutile, brookite and anatase. Anatase form of TiO_2, with band-gap energy of

3.2 eV, has been believed to have a higher photocatalytic performance than rutile, while brookite gives the least performance. Research has identified that most landmarks in photocatalysis were through the use of TiO_2 (Li *et al*., 2016a). As applied to all the semiconductor photocatalysts, TiO_2 exhibits photoexcitation, charge separation and surface reactions in a normal photocatalytic process. Consequent to that, improved TiO_2 photocatalysis can be accomplished by fine-tuning the material to influence each step and several modification methods have been explored. Surface modification was initially confirmed to be effective. Noble metals such as Pd, Pt, Au, Ag, and Rh can be incorporated on the surface of TiO_2 (Sakthivel *et al*., 2004). Hence, electron/hole charge separation can be enhanced for improved photocatalysis.

Surface or dye sensitization refers to the ability of an organic sensitizer to absorb more photons for activating and injecting more electrons to the semiconductor to obtain an improved efficiency. It has been reported that various dyes, such as thionines, erythrosin B, and different $Ru(bpy)_3^{2+}$ compounds can be applied as efficient sensitizers to trap sunlight for photocatalysis (Cho *et al*., 2001).

Integrating another lower band-gap semiconductor to TiO_2 could combine the benefits of surface modification and sensitization by trapping additional photons and as well suppressing the recombination of photoinduced electron/hole charges. According to Spanhel *et al*. (1997), it has been established that illuminated Cadmium sulfide (CdS) can transfer electrons to the integrated TiO_2, signifying a newly formed visible light response. Moreover, it has also been reported that metal sulfides such as WS_2, CdS, and MoS_2 and several metal oxides can improve the efficiency of TiO_2 response to visible light (Wu *et al*., 2006).

Compositional fine-tuning which is referred to as heteroatom doping is also anticipated to produce an outstanding influence on TiO_2 photocatalysis. At the outset, transition metal ions

were widely used as modifiers for TiO_2. The addition of metal ions can result to the creation of new band gap energy levels and decline in the recombination speed of the electron-hole pairs (Li *et al*., 2016). Despite the fact that a number of studies on transition metal (Xu *et al*., 2002) or rare earth modified titania had been carried out and reported, several setbacks associated with the use of metal doping have also been reported (Akpan and Hameed, 2010). For example, the thermal stability of the doped ions is poor. Also, the newly created energy bands can act as recombination centres, thus, resulting to reduced quantum efficiencies (Li *et al*., 2016b).

Non-metal functionalized TiO_2 has attracted far-reaching interest because of the induced visible light photocatalysis, which can make use of 42 % solar spectrum energy compared to less than 4 % of ultraviolet light (UV). The synthesis and application of nitrogen-doped TiO_2 in visible light photocatalysis has as well been reported by Asahi *et al*. (2001). Motivated by this outstanding work, several investigations on nitrogen doping have consequently been conducted and reported (Sun *et al*., 2008). With respect to heteroatom doping, co-doping with metals with nitrogen (Sun *et al*., 2013) or non-metals (Xiang *et al*., 2011) have been examined. The photocatalysis of Carbon doped titania has been also explored. Khan *et al*. (2002) established that carbon doped titania exhibited an improved absorption to visible light and the C-doping gave rise enhanced photocatalysis. Carbon-doped TiO_2 photocatalysts synthesized by several methods and their various applications (Ren *et al*., 2007) in addition to the co-doping studies with other elements (Chen *et al*., 2007) were subsequently reported. In addition to nitrogen or carbon doping, several elements such as, phosphorus (Asapu *et al*., 2011), sulfur (Li *et al* 2007), halogen elements (Sun *et al*., 2010) and boron (Zaleska *et al*., 2008), were also used to produce visible-light-driven TiO_2 photocatalysts.

2.5.1.2 ZnO and other metal oxide photocatalysts

ZnO has characteristic band-gap energy of 3.3 eV, which is close to that of anatase TiO_2, and has also been proven to be an efficient photocatalyst (Sun *et al*., 2014). In effect, ZnO could has demonstrated higher photocatalytic activity than TiO_2 (Sun *et al*., 2014), however it has poor stability which is attributed to photo-corrosion (Zhang *et al*., 2009). In order to enhance the stability, improving photocatalytic activity, and expanding the absorption of light in the visible region, different modifications, such as non-metal coupling (Rehman *et al*., 2009), semiconductor doping (Uddin *et al*., 2012), transition metal (Rekha *et al.*, 2010), or noble metal (Sun *et al.*, 2011), have been utilized. Other than the most known photocatalysts of TiO_2 and ZnO, several other metal oxide semiconductors have been successfully applied in photocatalysis. Hou *et al*. (2006) reported the effectiveness of β-Ga_2O_3 in photodegradation of gaseous benzene in air under UV light. Wang *et al*. (2012) studied the photocatalytic performance of Ga_2O_3 for water splitting, which can be significantly improved by adjusting the α-β junction. Faust *et al*. (1989) initially reported a successful photocatalytic oxidation of SO_2 in water using α-Fe_2O_3 photocatalyst. More investigations showed that it can be a possible photocatalyst for water splitting and organic pollutants degradation through photocatalysis (Pradhan *et al*., 2013). With respect to the low band-gap energy and the negative conduction band level, Cu_2O has been engaged as an effective photocatalyst for photoreduction in the splitting of water for hydrogen production (Xu *et al*., 2008). Various metal oxides such WO_3 (Kim *et al*., 2010), Bi_2O_3 (Zhou *et al*., 2009), and Ta_2O_5 (Sun *et al*., 2014), have shown good photocatalytic performances in a variety of applications.

2.5.1.3 Complex metal oxides and single-site photocatalysts

Integrating two or more metals in semiconductors would make it easier to transform the band structures such as band-gap energy, valence band (VB) level and that of the conduction band

(CB), thereby obtaining an improved photocatalysis. Some compounds, such as Zn_2GeO_4, $CaBi_2O_4$, $BiWO_6$ and $AgInW_2O_8$ have been synthesized by Liu *et al*., (2010)**.** When the detached and tetrahedrally arranged metal oxide moieties such as Mo, W, Cr, Ti, or V oxides, are infused into the silica-based zeolites or related permeable materials, single-site photocatalysts can be formed (Kim *et al*., 2010). Anpo *et al*. (2009) developed V-, Ti-, and Cr-oxide single-site photocatalysts and isolated them within zeolite frameworks. Their photocatalytic performances were investigated in the decomposition of NO or CO_2 conversion and the novel photocatalysis mechanism were as well discussed. Lately, metal-organic frameworks (MOFs) photocatalysts have also been developed; however, the challenges associated with poor stability are still needed to be addressed by further studies (Gao *et al*., 2014).

2.5.1.4. Metal sulfides and nitrides (or oxynitrides)

In pursuit for visible light photocatalysts that can serve as substitutes for wide band-gap metal oxides such as TiO_2 and ZnO, metal sulfides have been adopted as suitable alternative photocatalyst materials. Cadmium sulfide (CdS) which has suitable low band-gap energy of around 2.4 eV can utilize visible light with an absorption threshold at about 520 nm (Bao *et al*., 2008). Zong *et al*. (2010) established that under visible light photocatalysis using sulfite anion as a hole scavenger, CdS can generate hydrogen from water. In the photocatalysts for hydrogen production, CdS has most often been applied in the form of hybrid to avoid the problem associated with photo-corrosion (Park *et al*., 2008). The photodegradation of organic pollutants in wastewater has also been achieved using CdS when properly modified (Yu *et al*., 2014). Due to the quick creation of electron-hole pairs and its exceptional reduction potential for hydrogen formation and CO_2 conversion, ZnS has been confirmed to be a good photocatalyst (Hu *et al*., 2005). Photodegradation of organic pollutants in water using ZnS was also investigated

(Pouretedal *et al*., 2012). In the same way, various metal sulfides such as Ag_2S (Meng *et al*., 2012), NiS (Guo *et al*., 2013), CuS (Basu *et al*., 2010), In_2S_3, WS_2 (Sang *et al*., 2015) and some complex sulfides such as $A_2(I)$-Zn-A(IV)-S_4 [where A(I) = Cu and Ag; A(IV) = Sn and Ge] (Tsugi *et al*., 2010), $CuInS_2$, and $Zn_{1-x}Cd_xS$ (Li *et al*., 2013) have demonstrated their photocatalytic performances in a variety of photocatalytic reactions. Hitoki et al. (2002) reported that Ta_3N_5 can be an efficient visible light response photocatalyst capable of producing hydrogen and oxygen from water splitting. Ma *et al*. (2012) observed an improved water oxidation on a Ta_3N_5 photocatalyst which was enhanced by alkaline metal salts. Lee *et al*. (2006) reported that Ge_3N_4 can be applied for general water splitting. Moreover, metal oxynitrides, such as TaON and $Zn_xTiO_yN_z$ have also been investigated as visible light active photocatalysts (Gao *et al*., 2011).

2.5.1.5. Noble metal-based plasmonic photocatalysts

A number of novel photocatalysts appeared to initiate further exploration of photocatalysis mechanism. Tian and Tatsuma (2005) carried out the Plasmon-induced photo-electrochemistry in the visible light region on Au-TiO_2 composites, and observed that gold nanoparticles can be photo-excited due to the surface Plasmon resonance (SPR). The electron-hole charge separation can occur when the electrons are transferred from gold nanoparticles to the TiO_2 conduction band, and consequently the induced photocatalyst can oxidize organic pollutants (Tian and Tatsuma, 2005). Chen *et al*. (2016) developed several metal oxide-supported Au nanoparticles, such as Au/SiO_2, Au/Fe_2O_3, Au/CeO_2 and Au/ZrO_2, and enhanced photodegradation of gas pollutants was obtained under sunlight irradiation. Wang *et al*. (2009) reported the synthesis of Ag@AgBr and recommended it as a highly active plasmonic photocatalyst whose photo-response falls within the visible light region. An *et al*. (2010) proposed the facile synthesis of AgCl:Ag plasmonic nanoparticles as effective photocatalysts. The synthesized nanomaterials

exhibited improved degradation of organic pollutants present in wastewater under sunlight, and the enhanced performance was attributed to the strong SPR of metallic Ag components. The plasmonic photocatalysis can also be employed for degradation, hydrogen production, and chemical synthesis (Chen *et al*., 2016).

2.5.2 Metal-free Photocatalysts

The commonly reported metal free based photocatalyst is graphitic carbon nitride which is discussed in section 2.5.2.1.

2.5.2.1 Graphitic carbon nitride (g-C_3N_4)

The scarcity in nature and toxic metal leaching from photo-corrosion were considered to be the major impediments of metal-based photocatalysts to practical applications (Sun *et al*., 2014). A non-metal or metal-free photocatalyst, for example, graphitic carbon nitride (g-C_3N_4), has been recommended to be a possible substitute. Polymeric graphitic carbon nitride constitutes only non-metal, earth-abundant elements of carbon, nitrogen and hydrogen (Lotsch *et al*., 2007). It has been recognized as the most stable allotrope of carbon nitride, owing to the related layered shape to graphene. Carbon nitride has exhibited widespread relevance in a variety of catalytic reactions (Wang *et al.*, 2012). g-C_3N_4 is a polymeric semiconductor with the characteristic band-gap energy of 2.7 eV, distinctive structure and outstanding physicochemical properties (Groenewolt and Antonietti, 2005). Wang *et al*. (2009) for the first time observed efficient hydrogen production from visible light photocatalysis on g-C_3N_4 and the quantum efficiency was 0.1% under the irradiations in 420 – 460 nm. The low performance can be attributed to several factors, such as the high excitation energy, the low charge mobility of the polymer compared to metals or oxides, the low surface area ($\leq$10 m^2/g), and poor light absorption in extended wavelengths (Zhang *et al*., 2011). Consequently, several modification methods have been

employed to enhance the photocatalytic performance. Shalom *et al*. (2013) developed an ordered, hollow carbon nitride structure with the use of cyanuric acid melamine composite as the precursor. Improved photocatalysis for organic pollutants degradation was then achieved.

2.6 Synthesis of Graphitic Carbon Nitride

Graphitic carbon nitride can be prepared by chemical or physical method as discussed in sections 2.6.1. and 2.6.2

2.6.1 Chemical Process

The g-C_3N_4 nanostructure synthesis was pioneered by Xinchen Wang (Wang *et al*. 2009). They have used chemical route for synthesis. In chemical approach, the graphitic-C_3N_4 nanostructure is synthesized by thermal polymerization of nitrogen enriched precursors such as cyanamide, melamine, urea, thiourea (Figure 2.3) Thermal polymerization is the combination of poly-addition and poly-condensation. With increasing temperature, the precursors are usually condensed as their higher forms and at ~550°C temperature finally the tri-s-triazine based g-C_3N_4 is formed. Well-crystallized graphitic carbon nitride nanocrystallites also can be prepared via benzene-thermal reaction between $C_3N_3Cl_3$ and $NaNH_2$ at 180–220 °C for 8–12 h (Gou *et al*. 2003).

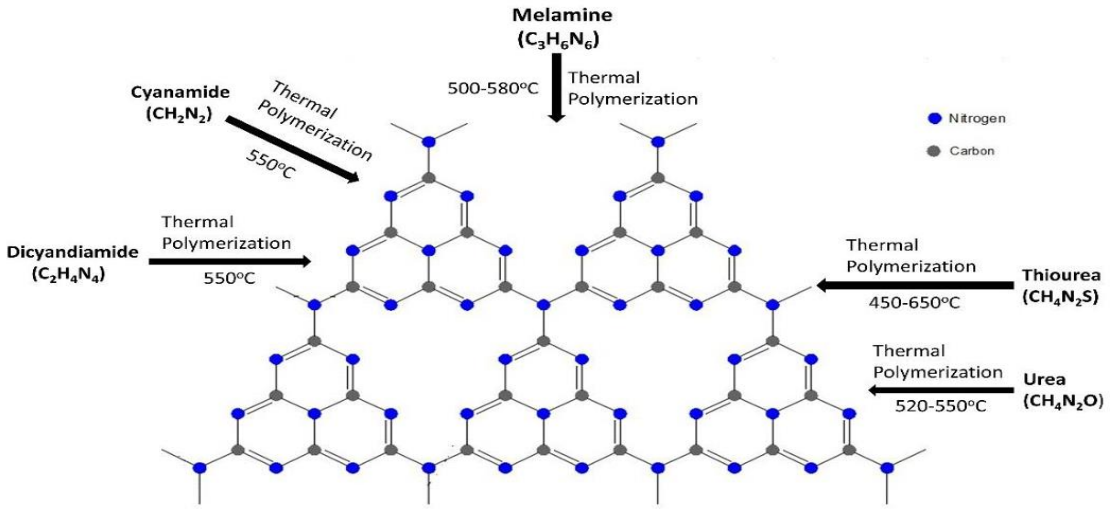

Figure 2.3: Schematic Illustration of g-C_3N_4 Synthesis by Thermal Polymerization Method (Wang *et al*. 2009).

2.6.2 Physical Process

The synthesis of graphitic-C_3N_4 nanostructure by sputtering method was performed by Guan *et al*, (2014). They synthesized g-C_3N_4 nanocone (g-CNNC) array by direct current (DC) plasma sputtering process. The Si substrate was polished with diamond powder. It was a two-step process. In first step, 100 nm thick Ni catalyst was deposited on polished Si substrate by ablating N_i target using Nd:YAG laser source under 7.5 µtorr vacuum pressure. In the second step, the Ni coated Si substrate was put on a graphite supporter as cathode, 0.5 cm below the conical shaped anode. The precursor gas mixture of CH_4 :(N_2+H_2) was inserted into the chamber maintaining a total pressure of 5.62 torr. A DC plasma was generated above the substrate through DC glow discharge. In the DC discharge plasma, precursor mixture was dissociated and CH_x radicals, H^+ ions and N^+ ions were formed. Here, CH_x radicals and H^+ ions had an important role for generation of g-CNNC. CH_4 did not contribute its C atom to form CN structure. The main role of H^+ ion is to sputter graphite frame to generate C atoms for

development of g-CNNC structure and another role is to etch graphite and amorphous carbon structure grown on Si substrate. In absence of CH_x radicals a large amount of C atoms were generated by H^+ ion sputtering which eventually develop Diamond nanocone (DNC). The bond dissociation energy of H_2 atom and CH_x radicals are nearly same (4.3-4.6 eV). So, in presence of CH_x radicals, they react with H atoms to form CH_4, maintaining a ratio of ~0.75 between C atom and N atom to generate C_3N_4 structure.

2.7. Structure of g-C_3N_4 Nanoparticles

It has been predicted on the basis of density-functional theory (DFT) that the g-C_3N_4 has two potential allotropes (i.e. triazine and tri-s-triazine structures) as shown in Figure 2.4 and the tri-s-triazine based structure is more stable (Kroke *et al*., 2002). The g-C_3N_4 spheres with tri-s-triazine structure have been synthesized by Thomas *et al* (Thomas *et al*., 2008) and Wang et al (Wang *et al*., 2009).

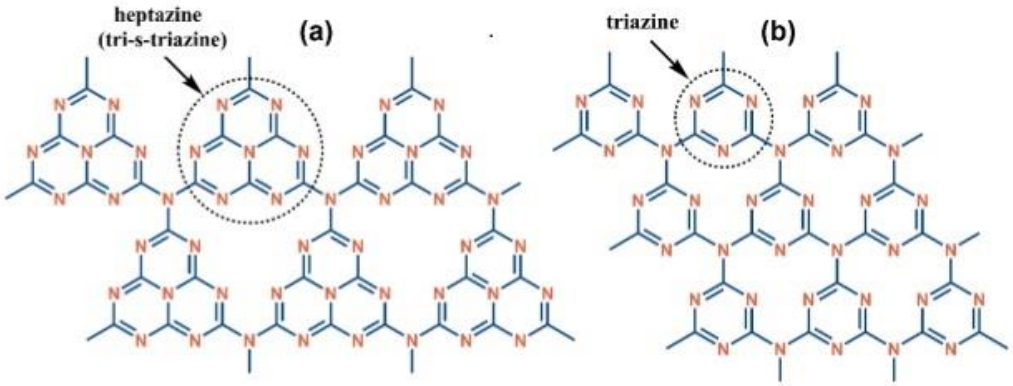

Figure 2.4: Structure of g-C_3N_4 based on (a) heptazine unit and (b) triazine unit (Kroke *et al.*, 2002)

2.8 Applications of Graphitic Carbon Nitride

The applications of g-C_3N_4 in catalysis have been extensively investigated in recent years, and it is now established as shown in Figure 2.5 that g-C_3N_4 is a good catalyst for a wide variety of reactions. The application of g-C_3N_4 in photocatalysis is one of the most current research topics worldwide, which is described based on the achievements mentioned in the literature (Zhu *et al.*, 2014)

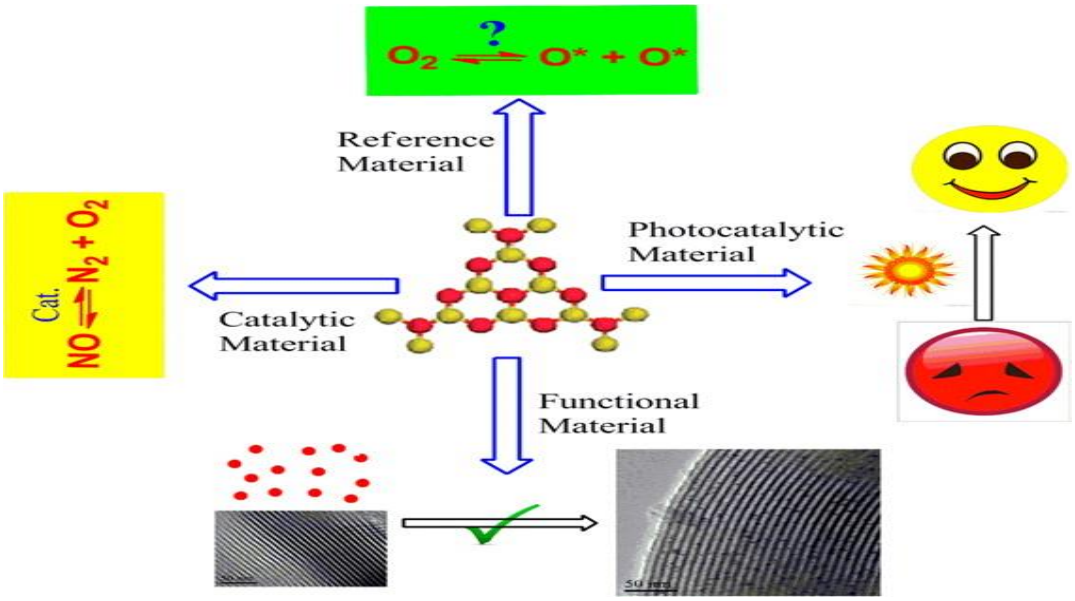

Figure 2.5: Applications of g-C_3N_4 (Zhu *et al*., 2014)

2.8.1 Metal-Free catalyst for NO decomposition

Nitrogen monoxide (NO) is a hazardous pollutant that causes environmental problems, such as acid rain and urban smog, and its removal is a challenging task nowadays (Zhu and Thomas, 2009). Direct decomposition of NO into N_2 and O_2 (Equation 2.9) is an ideal route for NO removal, as no reductant is needed and the products are the nontoxic N_2 and O_2.

$$2NO \rightarrow N_2 + O_2 \qquad 2.9$$

However, this reaction route is not yet carried out in industry since current inorganic catalysts encounter many problems when operating in real conditions. Another problem is that gaseous oxygen in the reacting atmosphere has negative effects on the reaction, namely: (1) it suppresses the desorption of atomic oxygen (formed in NO dissociation) from the active sites, making their regeneration difficult and thus poisoning the catalyst, (2) it competes with NO on the surface oxygen defects (active sites) during the adsorption process, preventing NO adsorption and activation on the catalyst surface and thus decreasing the activity (Zhu *et al*., 2007). g-C_3N_4 has strong resistance to oxygen and electron-rich properties (surface basic sites), being a suitable catalyst for NO decomposition. In addition, the polar C−N−C groups of g-C_3N_4 can also provide ideal adsorption sites for NO (that is a polar molecule).

2.8.2 Reference material to differentiate O_2 activation site

Catalytic oxidation is one of the most important reactions in industry and in our daily life. Molecular oxygen is the preferred oxidant due to its easy availability, low cost and nontoxicity. As O_2 molecule is not very active, it should be activated and dissociated into atomic oxygen before participating in the reaction (Sokolovskii, 1990). An effective and simple way for

clarifying the oxygen activation pathway over supported catalysts is the use of an oxygen-free and oxygen-inert support as a reference, so that the activation of molecular oxygen, if happening, can only proceed on the metal NPs. However, oxygen-free materials (e.g., carbon or metal nitride) are usually unstable in the presence of oxygen, and are easily gasified or oxidized at high temperatures, making them unsuitable for catalytic oxidations. Hence, g-C_3N_4 is useful as it is not only an oxygen-free and oxygen-inert material but also has high thermal stability even in oxygen atmosphere. Therefore, it can be inferred that if g-C_3N_4 supported metal catalysts are active for oxidation reaction using oxygen as oxidant, the oxygen must be activated on the metal sites. Thus, this principle can be used to test if the activation of molecular oxygen occurs on metal sites or on a support, by replacing that support by g-C_3N_4, and comparing the obtained activities.

2.8.3 Functional material for further preparation of small and stable nanoparticles

Nanocatalysis is one of the most exciting subfields of nanoscience, which aims to prepare nanoscale catalysts to control the activity and selectivity of reactions (Zhu and Zaera, 2014)**.** It is generally accepted that catalysts prepared in the nanoscale show enhanced catalytic performances than those in bulk, due to the quantum confinement effects (Alivisatos, 1996). However, ensuring the stability of the supported NPs and preventing their agglomeration and ripening in the reaction is still a complicated task (Zhu *et al*, 2013). The preparation of nanoscale catalysts with high stability is of interest, as it can not only broaden their applications, but also increase their durability. A good support should not only have high surface area to disperse the NPs, but also strong affinity for them, preventing their movement or leaching during the reaction. Interestingly, it was found that the particle size of metal NPs can be controlled, using supports with different loading or thickness of the CNx layer.

2.8.4 Metal-Free catalyst for photocatalysis

Compared to the conventional thermal catalysis, semiconductor photocatalysis is another efficient technology which uses the photons energy to activate the catalyst and subsequently, to catalyze the reaction. The solar energy is an endless and environmentally friendly source, which makes photocatalysis using g-C_3N_4 an attractive technology for solving environmental and energy problems, such as water contaminants degradation, water splitting, CO_2 reduction, and other chemical synthesis (Zhu *et al*., 2014). One challenging problem of this technology is to search for a suitable material that can efficiently harvest the photons, especially those from the visible light range.

2.9. Modification Routes for Graphitic Carbon Nitride (g-C_3N_4)

In general, g-C_3N_4 is a medium energy band gap semi-conductor with good visible light response (up to 460 nm). This suitable band gap, together with low cost, high chemical stability, ease of preparation, and pollution-free feature, is particularly sufficient for applications in photocatalytic organic pollutants degradation, CO_2 reduction, water splitting, and organic synthesis under visible light irradiation (Ong *et al*., 2016). However, the pristine g-C_3N_4 is commonly limited by insufficient photocatalytic performance due to the insufficient solar light absorption, low surface area and the rapid recombination of photogenerated electron-hole pairs (Mamba and Mishra, 2016).

In general, every photocatalytic reaction process would engage three sequential stages: photon absorption, electron–hole charges generation and separation, and catalytic surface reactions (Tachibana *et al*., 2012). Thus, a variety of modification strategies, such as elemental and molecular doping (Zhou *et al*., 2016), integrating with conductive materials (Zhao *et al*., 2015),

exfoliation to two-dimensional (2D) nanosheets (Lin *et al*., 2015), nanocomposite structure synthesis with other semiconductors (He *et al*., 2015), development of mesoporous g-C_3N_4 (Shi *et al*., 2015), and dye sensitization (Fang *et al*., 2016a) are employed to improve the photocatalytic performance of g-C_3N_4.

Wang *et al*. (2012a) reviewed the techniques for modulating the band structures of g-C_3N_4 by doping and copolymerization as well as other methods of producing permeable structures. The performance of the photocatalyst nanomaterials were evaluated in photochemical splitting of water and several reactions of organic oxidation and dehydrogenation. Zheng *et al*. (2012) developed a technique on the synthesis of g-C_3N_4 with tunable morphologies and structures, and discovered the promising future for environmental remediation. The synthesis of g-C_3N_4 and its applications as a metal-free catalyst for NO decomposition, a functional material for nanomaterial synthesis, a support for differentiating oxygen activation sites, and a photocatalyst, was presented by Zhu *et al*. (2014). A review on synthesis and modification of tailored g-C_3N_4 photocatalysts mainly for water splitting was reported by Zheng *et al*. (2015). Heterostructure construction, nanostructure design, crystal-structure engineering, and Electronic structure tuning were examined and discussed. Zhao *et al*. (2015) classified g-C_3N_4-based nanocompsites to be: g-C_3N_4/single metal oxide (sulfide), g-C_3N_4/composite oxide, g-C_3N_4/halide, g-C_3N_4-based complex system, g-C_3N_4/noble metal, and metal-free heterojunction. Cao *et al*. (2015) reported the design and synthesis of g-C_3N_4-based photocatalysts, with the improvement of pristine g-C_3N_4, bandgap engineering, and g-C_3N_4-based semiconductor complexes. The attention was particular on the improved photocatalysis by carbon materials, Z-scheme heterojunctions and non-noble-metal co-catalysts. Dong and Cheng, (2015) reported the exfoliation techniques for synthesis of two-dimensional g-C_3N_4 nanosheets, such as chemical exfoliation, thermal oxidation

exfoliation and ultrasonic exfoliation. Zhang *et al*. (2015) reviewed several synthesis techniques for g-C_3N_4 nanosheets, for example, top-down delamination and bottom-up assemblage of molecular building units. Ying, (2015) concentrated on the developments in enhancing the hydrogen production performance by loading noble metal free co-catalysts, exfoliation, and their extensive usage in photocatalytic O_2 evolution and CO_2 reduction. The structural modification of g-C_3N_4 using hard (carbon, anodic alumina oxide, silica) or soft templates (gas bubbles, surfactants and block copolymers, and ionic liquids) or biotemplates was the main focus of the study carried out by Yang *et al*. (2015). These methods could be applied to modify g-C_3N_4 for efficient photocalytic performance.

2.9.1 Structural modification

The structural modification of graphitic carbon nitride can be further categorized into the following

2.9.1.1 Hard templating

Hard template is a rigid material whose stable structure directly determines the size and morphology of sample particle. It has been established that a higher specific surface area (SSA) of catalysts can offer more active sites on the surface for improved catalysis. For pristine g-C_3N_4, it is regrettable that the surface area is normally lower than 10 m^2/g. Modification on g-C_3N_4 started with the formation of porous structure and the enhancement of SSAs. Hong *et al*. (2012) utilized SiO_2 nanoparticles as the hard template and achieved mesoporous g-C_3N_4 with an improved surface area of 128 m^2/g, while the unmodified one exhibited a low BET around 12 m^2/g. Zhao *et al*. (2014) reported the modification of mesoporous carbon nitride nanorods using SBA-15 as the template and hexamethylenetetramine as the precursor. A super enhanced specific surface area of 971-1124 m^2/g and an increased pore volume of 1.31-1.79 cm^3/g were obtained.

In another discovery, calcium carbonate was employed as a template to produce porous g-C_3N_4, and the obtained BET was 31.8 m^2/g, which is about three folds more than the pristine one. Furthermore, about 4 – 7.5 times increase in photocurrent was obtained (Wang *et al*., 2015). Liang *et al*. (2015b) presented a macroscopic 3D porous g-C_3N_4 monolith by the method of thermal polymerization of urea contained in a unique template of melamine sponge (MS), usually obtained in the kitchen. The specific surface area (SSA) and pore volume of the material were observed to be 78 m^2/g and 0.76 cm^3/g, respectively. Sequel to the fabrication of silica-templated g-C_3N_4 to be applied for hydrogen evolution, Li *et al*. (2015) proposed that the limitation of the photoactivity of g-C_3N_4 is as a result of the sluggish charge mobility just like other polymeric semiconductors, and thus, the structure reformation should be advantageous for the enhanced electronic properties.

2.9.1.2. Soft templating

Pluronic P123 was employed as a soft template to synthesize g-C_3N_4 with a resultant worm-like pore and constricted pore size distribution and the BET surface area was improved from 10 m^2/g to 90 m^2/g (Yang *et al*., 2015). The synthesis of a sponge-like form of graphitic carbon nitride through the method of biopolymer-activation via soft-templating with the use of seaweed polysaccharide or gelatin was reported by Zhang *et al*. (2013). The control material of pristine g-C_3N_4 had a low BET of 10 m^2/g, whereas 6 folds higher BET (63 m^2/g) was obtained by the soft-templating process. The increased BET can enhance the photoelectrochemical performance, nevertheless, the sample having the highest BET does not guarantee the highest activity. This is because the increase of surface area of g-C_3N_4 can sometimes lead to the deterioration of crystalline formation with more defects, which will lead to increased recombination of photoinduced electron/hole pairs. Moreover, it was observed that soft-templating modified

samples exhibit a relatively inferior BET value than those obtained through hard-templating process.

2.9.1.3. Template-free

Han *et al*. (2013) reported that the BET of g-C_3N_4 can be increased to 210 m^2/g by a facile template-free method controlling the reaction of polymer according to Le Chatelier's principle. In the synthesis, a semi-closed system was applied to make the polymerization partially expose to air. The partial oxidation can also be employed as post-treatment of g-C_3N_4. Niu *et al*. (2012) reported that the BET of g-C_3N_4 can be increased to 306 m^2/g when it was exfoliated to nanosheets by a simple top-down method of thermal oxidation etching of bulk g-C_3N_4 in air. Manipulation of the synthesis without a template appears to be effective for improving the textural properties of g-C_3N_4. Recently, mesoporous g-C_3N_4 nanomesh with the atomic thickness was fabricated by solvothermal exfoliation of the mesoporous sample (Han *et al*., 2016). It was found that the structural modification can effectively tune the energy levels, charge mobility, light absorption, and surface active sites. With the modified properties, the prepared g-C_3N_4 nanomesh was able to continuously produce hydrogen from water for 30 h at a rate of 8510 μmol/h/g, under visible light of $\lambda > 420$ nm. The activity was 5.5 times higher than that of bulk counterpart, and 24.3-fold as compared to traditional bulk carbon nitride. She *et al*. (2016) reported the template-free synthesis of 2D porous ultrathin g-C_3N_4 nanosheets. The enhanced photocatalytic performances were shown in both photocatalytic water splitting and photodegradation at 5.2 and 71 times higher, respectively. Introducing salts in the synthesis has been proven to be effective for the creation of porous structure of g-C_3N_4. Ma *et al*. (2016) developed an in situ ion-assisted synthesis of porous g-C_3N_4 nanosheets, in which lithium chloride was used to produce a porous sample with 2-3 nm pores and 2-3 nm thickness, and a high surface area of 186.3 m^2/g. It can be seen that all the soft- or hard-templating and template-free approaches can be applied to prepare porous g-C_3N_4 with enlarged BET and pore volume.

Because of the mechanical strength and stability in the polymerization process of g-C_3N_4 precursors, generally hard-templating can produce better textural properties than soft-templating and template-free protocols. The improved porous structure from the structural modification will be able to enhance the adsorptive, photocatalytic and photoelectrochemical properties of g-C_3N_4 materials. It is noteworthy that the normalized performance (to surface area) of the porous g-C_3N_4 is usually low than pristine g-C_3N_4. This is different from metal-based catalysts. It was suggested that the key parameter of g-C_3N_4 in determining the photocatalytic activity is not the surface area and pore volume, but the charge mobility and separation rate (Li *et al*., 2015). Lin *et al*. (2016) reported that the crystalline g-C_3N_4 with tri-s-triazine subunits derived from the tri-s-triazine-based precursor and the salts of KCl and LiCl would possess the improved crystallinity and enhanced charge carrier mobility, and then showed higher photocatalytic hydrogen production.

2.9.2. Shape-control synthesis

In metal-based catalysis, for example, involving noble metals (Zhang *et al*., 2013) and metal oxides (Sun *et al*., 2013), it has been well established that the shape of the catalyst represents the exposed crystal facet, which can be a key parameter for manipulating the catalysis performance. In the synthesis of g-C_3N_4, in addition to 2D nanosheets, a number of other shapes were fabricated. Liu *et al*. (2014) reported that uniform g-C_3N_4 nanorods (200 nm long and 80 nm wide) can be fabricated by a morphology-preserving route using SiO_2 nanorods as the template. The BET surface area of the nanorods was determined to be 52 m^2/g, about two times higher than the bulk g-C_3N_4. Blue-shift and suppressed charge recombination were observed on the nanorods. Transformation of g-C_3N_4 nanorods from nanoplates was carried out by a simple reflux method (Bai *et al*., 2013). Since the BET was not significantly increased, the enhanced

photocatalysis was ascribed to the increase of active lattice face and the removal of surface defects.

Graphitic carbon nitride (g-C_3N_4) nanospheres composed of nanosheets were prepared by a templating route using KCC-1 silica spheres as sacrificial templates (Zhang *et al*., 2014). A high BET surface area of 160 m^2/g for the nanospheres was obtained compared to 9 m^2/g of bulk g-C_3N_4. Excellent photocatalytic hydrogen evolution was observed owing to the improved mass transfer and better charge separation originated from the structural benefits. Template-free synthesis of g-C_3N_4 microspheres was developed using a solvothermal method with melamine and cyanuric chloride as the precursors (Ma *et al*., 2016). The porous structure, narrowed band gap and lowered resistance were proposed to the origins of the enhanced H_2 production. Jun *et al*. (2013) reported the synthesis of carbon nitride hollow spheres by melamine-cyanuric acid supramolecular aggregation. Stronger optical absorption, widened band gap, an increase of lifetime of the charges worked together to achieved 10 times higher photodegradation over the g-C_3N_4 hollow spheres. Openly-structured microspheres of g-C_3N_4 with an ordered hierarchically porous structure, modified absorbance and electronic properties were prepared by Huang *et al*. (2016), and the photocatalysts demonstrated enhanced photocatalysis. Under λ>420 nm visible light irradiation, the best catalyst showed a hydrogen evolution rate of 392 μmol/h, as compared to 27 μmol/h on a bulk sample. Zheng *et al*. (2014) reported the preparation of helical g-C_3N_4 with a twisted hexagonal rod-like morphology via nanocasting with chiral SiO_2 templates. It was suggested that the helical nanoarchitectures are able to promote charge separation and mass transfer to obtain better water splitting and CO_2 reduction. It can be seen that the shape-control synthesis of g-C_3N_4 can be achieved with or without a template. Also, considerable crystalline structure changes were not observed and in general, the enhanced photocatalysis was suggested

to be from the structural benefits. This is the same as the creation of porous structure for g-C_3N_4. Moreover, improved charge transfer and mass transfer as well as tailored optical property were present in the morphology-controlled g-C_3N_4. Preferred exposed facets for enhanced catalysis on metals or metal oxides is not the case here (Sun *et al*., 2013).

2.9.3. Heteroatom doping

This involves the doping of the photocatalyst with materials such as metals and non metals as discussed in sections 2.9.3.1 and 2.4.3.2

2.9.3.1. Metal doping

Generally, the introduction of metallic impurities inflicts additional binding functions, which endows the doped system with unique photocatalytic properties by lowering the band gap and enhancing the absorption of visible light (Zheng *et al*., 2015). In order to import metal ions into the framework of carbon nitrides, the corresponding soluble salt is always uniformly mixed with the precursor of g-C_3N_4. In this way, metallic impurities will be simultaneously doped into the g-C_3N_4 framework during the thermal condensation process of precursor.

This technique has also been employed to modify g-C_3N_4. Fe-doped graphitic carbon nitride (g-C_3N_4) nanosheets were prepared by Tonda *et al*. (2014) using ferric chloride as the Fe-precursor. The Fe dopant appeared to be in +3 oxidation state and could significantly influence the electronic and optical properties of g-C_3N_4. It was reported that 2 mol% Fe-doped g-C_3N_4 showed almost 7-time and 4.5-time higher activity than unmodified g-C_3N_4 and g-C_3N_4 nanosheets, respectively.

Potassium-doped g-C_3N_4 was prepared by the thermal polymerization of dicyandiamide and KI. It was found that the doped potassium can enhance the photocatalytic activity by lowering the valence band and increasing charge separation rate (Zhang *et al*., 2015). Besides, Zr-doped and W-doped g-C_3N_4 were also developed for enhanced photocatalysis (Rong *et al*., 2016)

2.9.3.2. Non-metal doping

In consideration of the metal-free nature of the modified g-C_3N_4, non-metal doping has attracted more extensive interest. Moreover, as demonstrated in doped TiO_2 or other metal oxide photocatalysts, non-metal doping can also avoid the thermal variation of chemical states of doped metal ions (Sun *et al*., 2011).

Oxygen doping: Following the idea of heteroatom doping, a variety of dopants of non-metal elements have demonstrated the great effectiveness for g-C_3N_4 based photocatalysis. Huang *et al.* (2015) reported that porous O-doped g-C_3N_4 was prepared by a precursor pre-treatment method forming hydrogen bond-induced supramolecular aggregates for the creation of the porous structure and tailored O-doping. The porous structure and O-doping worked together to achieve respective 6.1 and 3.1 times higher hydrogen evolution than bulk and porous g-C_3N_4 (non-doping). Guo *et al*. (2016) prepared holey-structured g-C_3N_4 with doped oxygen at the edges via photo-Fenton reactions. Lowered band gap energy of 2.43 eV and increased BET of 348 m^2/g were achieved. The effect of oxygen doping on the electronic and geometric structure of g-C_3N_4 was investigated by the first principle (Cui *et al*., 2015). It was theoretically confirmed that oxygen doping can improve the visible light absorption, increase the carrier mobility, produce more active sites and reduce the recombination of electron/hole pairs.

Sulfur doping: Zhang *et al*. (2011) developed the sulfur-mediated synthesis to stimulate carbon nitride bulk condensation by trithiocyanuric as the precursor in which the –SH groups were supposed to play a key role in adjusting the physicochemical properties of the prepared g-C_3N_4. A trace amount of sulfur doping showed effective modifications of the textural, optical and electronic properties. As a result, the activity in water oxidation reactions was improved. Liu *et al*. (2010) reported that sulfur-doping can induce a unique electronic structure that shows an increased VB along with an elevated CB minimum and minor declined absorbance. Significant changes in optical properties and electronic structures would lead to the enhanced photocatalysis in hydrogen evolution over the sulfur-doped g-C_3N_4, with 7.2 and 8.0 times higher than unmodified one under $\lambda > 300$ and 420 nm, respectively. Sulfur-doped g-C_3N_4 was also used for photocatalytic CO_2 reduction. Wang *et al*. (2015) reported that sulfur-doped g-C_3N_4 can convert CO_2 by photocatalysis to CH_3OH with a yield of 1.12 μmol/g as compared to 0.81 μmol/g on undoped sample. The first-principle studies showed that the band gap was not changed by the doping, however impurity states appeared. Stobov and Zuluga (2013) carried out a comprehensive first-principles study to investigate the effect of sulfur doping on the electronic and geometric structures of g-C_3N_4. It was found that sulfur would contribute to the valence charge densities and then significantly reduce the band gap energy. Other than the effect of sulfur-doping on the catalyst, Lin *et al*. (2015) applied DFT calculations to determine the influence of sulfur-doping on the reaction mechanism of photocatalytic water oxidation. They found that sulfur-doping to g-C_3N_4 not only induces a different reaction mechanism but also decreases the overpotential. The S-doped g-C_3N_4 photocatalysts have demonstrated effectiveness in photodegradation, H_2 evolution, CO_2 reduction and water oxidation. As various synthesis

routes were involved, some inconsistence raised in the studies might be due to the different chemical states of the dopants.

Phosphorus doping: Phosphorus-doped g-C_3N_4 was prepared by poly-condensation with the precursor of g-C_3N_4 (dicyandiamide) and a heteroatom source namely a phosphorus-containing ionic liquid. Phosphorus doping and structural modification were integrated by Ran *et al*. (2015), who prepared porous P-doped g-C_3N_4 nanosheets by combining P doping and thermal exfoliation of a bulk material. The P-doping and novel macroporous nanosheets morphology significantly increased the visible light photocatalytic H_2-production compared to pristine g-C_3N_4. The newly formed mid-gap states (-0.16 V vs. SHE) were observed due to the P-doping. With the similar strategy of simultaneous tailoring of texture and electro-/optical-properties, mesoporous P-doped g-C_3N_4 nanostructured flowers were also prepared by a co-condensation method in the absence of any templates (Zhu *et al*., 2015). Improved hydrogen evolution under visible light irradiation was observed due to the promoted light trapping, mass transfer, and charge separation. Guo *et al*. (2016) applied a hexagonal rod-like supramolecular as the precursor of g-C_3N_4 and phosphorous acid as a P source to prepare P-doped carbon nitride tubes and used the photocatalysts to carry out hydrogen evolution reactions. It was observed that, after P-doping, the band gap energy was decreased to 2.55 from 2.67 eV. Furthermore, 7 times higher photocatalytic H_2 evolution rate was achieved.

Iodine doping: Iodine-modified g-C_3N_4 was synthesized by the co-condensation of dicyandiamide and ammonium iodine. It was expected that the introduction of iodine can induce effective extension of aromatic carbon nitride heterocycle by Iodine ions. Extended optical absorption, reduced band gap energy, improved charge separation and enhanced hydrogen evolution were achieved (Zhang *et al*., 2014). Iodinated g-C_3N_4 nanosheets were prepared by a

simple and scalable method using a ball-milling technique (Han *et al*., 2016). Both photoelectrochemical and photocatalytic properties were changed by I-doping.

Fluorinated g-C_3N_4 was prepared by directly incorporating NH4F into the thermal condensation process in g-C_3N_4 synthesis (Wang *et al*., 2010). The doped F can shift both VB and CB to higher energy values, which were beneficial for the redox properties and could enhance heterogeneous photocatalysis.

Nitrogen, fluorine or boron doping: Nitrogen-doped g-C_3N_4 was fabricated by the co-thermal condensation of the precursor of melamine with a nitrogen-rich additive of hydrazine hydrate (Wang *et al*., 2015). Zhou *et al*. (2016) reported the synthesis of N-doped g-C_3N_4 using citric acid and urea as the starting precursors for the thermal polymerization. It was suggested that the lone pair electron on the graphitic N atom can result in the aromatic π-conjugated system being extended and delocalized. As a result, the performances of photocatalysis and photocurrent were improved. Boron-doped g-C_3N_4 was prepared by heating a mixture of melamine and boron oxide (Yan *et al*., 2010). It was found that boron doping for g-C_3N_4 can improve the efficiency of photodegradation of Rhodamine B (Rh B) owing to the increased dye adsorption and light absorption of the catalyst..

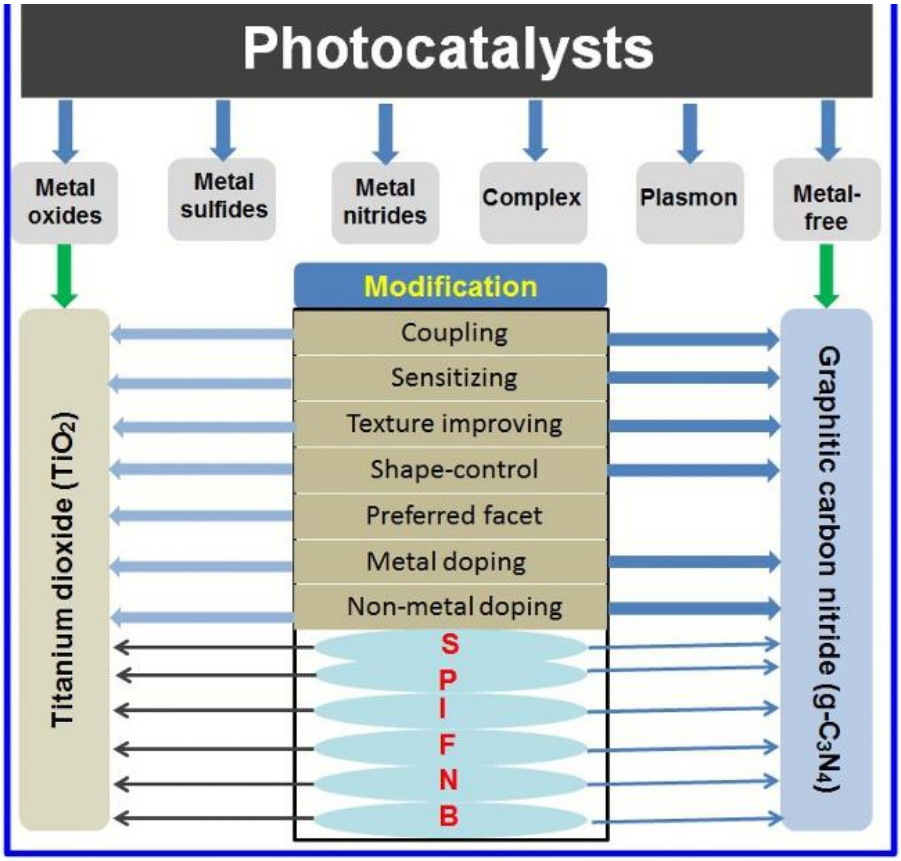

Figure 2.6: Development of Photocatalysts with the Focus on the Non-metal Modification of Graphitic Carbon Nitride (Sun et al., 2011).

Vacancy/defect modification: The defect and vacancy would profoundly influence the properties of the crystalline materials, thereby controlling the catalytic activity. Wu *et al*. (2016) used melamine to remedy various defects (for example, cyano and amino defects) of mesoporous g-C_3N_4. Once the defects were passivated, better separation and transfer of electron-hole pairs can be achieved. In the photo-oxidation reactions of 1,4-dihydro-2,6-dimethylpyridine-3,5-dicarboxylate (1,4-DHP) and the associated/simultaneous hydrogen production, the conversion and H_2 evolution of the remedied sample were enhanced 2 and 6.5 times than the unmodified mesoporous g-C_3N_4. Li *et al*. (2016) applied hot argon gas to create carbon vacancies onto g-

C_3N_4. Both experimental and theoretical investigations proved that the carbon vacancies would reduce the symmetry of the g-C_3N_4 and modulate the electronic structure. The vacancies would also make g-C_3N_4 have more excited electrons and lowered band gap energy. In the photocatalytic H_2O_2 production reaction, 14 times more production rate was achieved via the carbon-vacancy modification. .

2.9.4. Semiconductor coupling

This involves integrating external materials such as metal oxides and metal free materials into the crystal lattice of the photocatalyst for enhanced photocatalytic activity.

2.9.4.1. Coupling metal oxides

Coupling a semiconductor to another is an effective technique to create heterojunctions for the extended absorbance and improved charge separation, which could enhance the photocatalytic performances. Yan and Yang (2011) reported that coupling TiO_2 to C_3N_4 can remarkably increase the photocatalytic hydrogen evolution rate due to the improved charge separation efficiency. Li *et al*. (2015) prepared various TiO_2 nanostructures, such as 0D nanoparticles, 1D nanowires, 2D nanosheets, and 3D mesoporous nanocrystals and attached each of them onto g-C_3N_4 to create heterojunctions, respectively. Meso-TiO_2/g-C_3N_4 demonstrated the highest activity in the photodegradation of methyl orange (MO) and phenol, with 29-37 times higher than bare g-C_3N_4. He also reported the fabrication of g-C_3N_4/(0 0 1)-TiO_2 composite by a solvent-free in situ method. The compact connection between g-C_3N_4 and (0 0 1)-TiO_2 can facilitate the interfacial charge transfer process. Therefore, the photocatalytic activity was enhanced in removal of NO, with 2.4 times higher than pure (0 0 1)-TiO_2 and 4.1 times higher than g-C_3N_4 under UV, respectively.

Other metal oxides, such as α-Fe_2O_3, SnO_2, WO_3 and CuO (Wang *et al*., 2015) were also used to couple with g-C_3N_4. A variety of bimetallic oxides, such as $SnNb_2O_6$ nanosheet (Zhang *et al*., 2016), $NaNbO_3$ (She *et a*l., 2014), $CuFe_2O_4$ (Yao et al., 2015), and Ag_3VO_4 (Zhu *et al*., 2015) have been demonstrated to be effective for modification of g-C_3N_4. Besides, metal sulfides (Akple *et al*., 2015), metal oxohalides(Li *et al*., 2015), ternary compounds (Guo *et al*., 2016) and other novel materials such as phosphates (Liu *et al*., 2016), polyoxometalate (He *et al*., 2015), and zinc phthalocyanine (Lu *et al*., 2016) were also able to modify g-C_3N_4 for enhanced photocatalysis.

2.9.4.2. Metal-free hybridization

Carbonaceous materials: To maintain the metal-free nature, non-metal compounds were employed for modification of g-C_3N_4. Zhang *et al*. (2011) described non-covalent modification of g-C_3N_4 with graphene and suggested that, with the π – π stacking interaction, the band structure of g-C_3N_4 can be modulated for enhanced photoelectrochemical properties. Graphene oxide (GO) modified g-C_3N_4 was prepared by a sonochemical approach (Liao *et al*., 2012. Ge and Han (2012) prepared MWCNT/g-C_3N_4 composite as efficient visible light photocatalysts for hydrogen evolution from water. At the optimal modification level of 2.0 wt%, the composite photocatalyst showed 3.7 folds higher hydrogen evolution from methanol solutions than pristine g-C_3N_4. Sun *et al*. (2014) described an interesting, metal-free hybrid photocatalyst made of carbon nitride and carbon spheres. The prepared pristine g-C_3N_4 was hydrothermally treated with glucose, which was then converted to uniform carbon spheres attaching onto carbon nitride sheets. It was found that the introduction of carbon spheres significantly improve the optical absorption and charge separation. Enhanced photodegradation of organic pollutants was observed. A composite of g-C_3N_4/S-doped porous carbon was then prepared and its photoactivity

was investigated (Seredych *et al*., 2016). The material was determined to be conductive, porous and surface active due to the sulfur-functionality and then demonstrated excellent electroreduction under visible light.Very recently, carbon dots were used to fabricate g-C_3N_4 hybrid photocatalysts. Fang *et al*. (2016) prepared carbon dots modified g-C_3N_4 using C-dots and dicyandiamide as the starting materials. A series samples, S0, S4, S5, S6, and S10 (where 0, 4, 5, 6, and 10 referred to n mL of C-dots in the starting materials) were obtained and the C-dots loading levels were dependent on the initial volumes. The photocatalytic performances of the hybrid of C-dots and g-C_3N_4 were evaluated by both photodegradation of RhB under UV and hydrogen production under visible light irradiations. It was found that, S5 (0.25 wt% C-dots modified g-C_3N_4, via 5 mL C-dots as the precursor) showed the best activity in both the reactions. It was suggested that the C-dots would induce the lattice distortion, act as the electron-sink, and prevent the recombination of the photoinduced charges. However, a too high level of C-dots might form the recombination centre and then reduce the photocatalytic activity. Similar studies were also carried out by Li *et al*. (2016) using carbon quantum dots.

Polymeric materials: Grafting functional groups onto g-C_3N_4 can be obtained by copolymerization with organic compounds having amino group. Zhang *et al*. (2012) employed various monomer building blocks with desired compositions and electronic structures for modification of g-C_3N_4. Enhanced photocatalysis was claimed on the modified photocatalysts. Chu *et al*. (2013) reported a simple bottom-up approach to prepare g-C_3N_4 with a desired band structure by incorporating an electron-deficient pyromellitic dianhydride (PMDA) monomer. The modified g-C_3N_4 has a lowered VB ensuring stronger photo-oxidation ability in degradation of MO. Moreover, the formation processes of reactive radicals were tuned by photoinduced holes other than electrons due to the band gap engineering.

Other metal-free materials: Some other metal-free compounds, such as polyacylonitrile (g-PAN) (He *et al*., 2014), melem (Liu *et al.,* 2016) and g-C_3N_4 itself (Yang *et al*., 2016) were also employed to modify g-C_3N_4. In recent studies, Zhu's group prepared a 3D C_3N_4-agar hydrogel photocatalyst and C_3N_4/SiO_2 hydrogels (Zhang *et al*., 2016), and evaluated their photocatalytic activities. Ansari *et al*. (2016) reported the feasible synthesis of g-C_3N_4/red phosphorus and its potential applications for degradation of dyes and energy storage.

2.9.5. Dye-sensitization of g-C_3N_4

Dye sensitization was discovered a long time ago and has been widely used in photocatalysis and solar cells. With the light absorption and the injection of electrons from dye excitation, the solar energy conversion efficiency can be greatly increased. Takanabe *et al*. (2010) reported that magnesium phthalocyanine (MgPc) dye sensitization of mesoporous carbon nitride can lead to highly efficient hydrogen evolution even with irradiations longer than 600 nm. Highly asymmetric phthalocyanine (zinc-tri-PcN) was used to modify carbon nitride due to the intense near-IR light absorption (Zhang et al., 2016). In the photocatalytic hydrogen evolution reaction (HER), a very high quantum yield of 1.85% at 700 nm was achieved.

Zhang *et al*. (2015) reported that four commonly used xanthene dyes such as fluorescein, dibromofluorescein, eosin Y and erythrosine B were compared in dye-sensitization of carbon nitride. The electron transfer rate from the LUMO of the each excited dye to the CB of carbon nitride was investigated. Moreover, the possibility of the selected xanthane dye as a hole acceptor was discussed in the implications for photocatalysis. In a recent study, Liu *et al*. (2016) found that oxygen doping can promote the dye-sensitization process. With the tests employing four dyes, Eosin-Y, Perylene, Nile-red and Coumarin, Nile-red sensitization was effective for MB degradation while Eosin-Y was suitable for phenol degradation. However, without oxygen

doping, the dye sensitization was not effective. Fang *et al*. (2016) observed that the pre-treatment of the carbon nitride precursor would profoundly influence the resulting g-C_3N_4 samples. The optical and electronic properties were modulated and then enhanced hydrogen production was obtained compared to bulk g-C_3N_4.

2.9.6 Green Modification Technology

The green modification of photocatalysts by plants and phytochemicals is mainly advantageous due to its easy availability, simplicity, cost-effectiveness, relative reproducibility, production of stable materials, use of non-toxic chemicals, environmental friendliness, and higher efficiency. It does not require intense maintenance of laboratory cultures for NPs synthesis (Benelli *et a.,* 2017). Plant extract behaves as a reducing and capping agent, which controls the particle size and particle shape of Nanoparticles (Philip, 2010). The utilization of plant extracts as a reducing agent in lieu of conventional reducing agents (Citric acid $C_6H_8O_7$, Sodium Borohydride $NaBH_4$, Lithium aluminium hydride $LiAlH_4$, Nitric acid HNO_3) have led to a remarkable progress in green synthesis protocol for the synthesis of several nanaoparticles. Modern NPs synthesis using plant systems has gained heightened research interest for many investigators as it is highly economical and for the large-scale synthesis of NPs. Extracts from different parts of the plants, including leaf, root, latex, fruit pericarp, fruit juice, seed, and stem, have been used for the synthesis of NPs where they act as stabilizing and/or reducing agents (Borase *et al*., 2014). Researchers have synthesized NPs from various plant sources such as *Azadirachta Indica* (neem), *Ocimum tenuiflorum* (tulsi), *Eclipta prostrata* (false Daisy), *Jatropha cucas* (Barbados), *Rhododedendron daurican* (Midwinter), *Euchinacea purpurea* (purple coneflower)), *Ageratina altissima* (White snake root), *Habiscus rose-sinensis* (Habiscus flower) (Kumar *et al*., 2014). In general, the prominent role of polyphenols was observed in plant extracts used in nanosynthesis,

however, other biological constituents, such as alkaloids, carboxylic acids, glycosides, polyols, ascorbic acid, terpenoids, amino acids, tannins and flavonoids, were also involved in the reduction, capping, and stabilization of NPs (Borase *et al*., 2014)..

2.10 Neem plant (*Azadirachta indica*)

Azadirachta indica, commonly known as neem, nimtree or Indian lilac (Verma *et al*., 2016) is a tree in the mahogany family Meliaceae. It is one of two species in the genus Azadirachta, and is native to the Indian subcontinent like India, Nepal, Pakistan, Bangladesh, Sri Lanka, and Maldives. It is typically grown in tropical and semi-tropical regions. Neem trees also grow in islands located in the southern part of Iran. Its fruits and seeds are the source of neem oil. Neem is a fast-growing tree that can reach a height of 15–20 metres (49–66 ft). It is evergreen (plate I), but in severe drought it may shed most or nearly all of its leaves. The branches are wide and spreading. It can grow in regions with an annual rainfall below 400 mm, but in such cases it depends largely on ground water levels. Neem can grow in many different types of soil, but it thrives best on well drained deep and sandy soils. It is a typical tropical to subtropical tree and exists at annual mean temperatures of 21–32 °C (70–90 °F). It can tolerate high to very high temperatures and does not tolerate temperature below 4 °C (39 °F). Neem leaves are dried in India and placed in cupboards to prevent insects eating the clothes, and also in tins where rice is stored (Yashroy and Gupta, 2000). The tender shoots and flowers of the neem tree are eaten as a vegetable in India. Products made from neem trees have been used in India for over two millennia for their medicinal properties (Subapriy and Nagini, 2005). Neem products are believed to be anthelmintic, antifungal, antidiabetic, antibacterial, antiviral, contraceptive, and sedative (Maragathavalli *et al*., 2012). Neem oil is also used for healthy hair, to improve liver function, detoxify the blood, and balance blood sugar levels (Maragathavalli *et al*., 2012). Neem

leaves have also been used to treat skin diseases like eczema and psoriasis (Arshad *et al*., 2010). Phytochemical screening of neem leaves showed the significant presence of phenol, flavonoid and tannin (Pandey *et al*., 2014). The phytochemicals present in Neem leaves are mainly flavonoid and tannin, which act as reducing as well as capping agent and helping in stabilizing nanoparticles (Verma *et al*., 2016).

Plate I: ***Azadirachta indica*** **(Neem) leaf**

2.11 Local Dyeing Wastewater and its Environmental Impacts

Basically, Substances that add color to textiles when they are incorporated into the fiber by chemical reaction, absorption, or dispersion, are called dyes. They can be classified according to their applications and are used in the local dyeing industry (Chen *et al*., 2003). The common dyes applied in the textile industries are acid dyes, basic dyes, direct dyes, azo dyes, reactive dyes, mordant dyes, vat dyes, disperse dyes and sulfur dyes (Ghaly *et al.*, 2014). Wastewater from local dyeing industries is complex mixtures of chemicals varying in quantity and quality. Of a particular interest are organic and inorganic chemicals, which when released directly into

the water bodies, affect its chemical oxygen demand (COD) and biochemical oxygen demand (BOD) among others (Gupta, 2015). The discharge of this dyeing wastewater into the environment often produce a bad colour and can cause diseases such as hemorrhage, nausea, severe irritation of the skin and dermatitis, and can aslo block the penetration of sunlight into the water surface, thereby distorting the aquatic life (Nese *et al*., 2007). Local dyeing wastewater usually contain considerable amount of inorganic anions (such as nitrates, carbonates, sulphates and phosphates) amongst others, coexisting with organic contaminants. Inorganic anions have scavenging effect on the heterogeneous photo catalytic process, by changing the ionic strength of the reaction medium and inhibiting the catalytic activity of the photocatalyst (Ghaly *et al.,* 2016).

2.12. Characterization Methods

The different characterization techniques that can be used to investigate the properties of g-C_3N_4 nanomaterials are as follows: Scanning Electron Microscopy (SEM), energy Dispersive Spectroscopy (EDS), X-ray Diffraction (XRD), Fourier Transform Infrared Spectroscopy (FT-IR) and Brunauer Emmett and Teller (BET).

2.12.1. Scanning Electron Microscopy (SEM)

SEM is one of the useful imaging techniques that use a beam of electrons to form high low magnification images in order to provide information on the morphological arrangement of the particles in the material (Pappa *et al*., 2015). Tungsten and Lanthanum hexaboride filaments are mostly used as electron source with the cathode heated to supply electrons having energy of a few hundreds to 40 KeV (Havancsak, 2017). These electron sources have high melting points and relatively low work function, hence they are commonly used. The electron beam produced is accelerated by the applied voltage towards the anode, passes the anode via a magnetic lens system through an aperture into the vacuum chamber to the surface of the specimen. Image

formation is dependent on the produced signals from the electron beam and electron interaction with the specimen.

The deflection of electrons by the outer shell electrons or atomic nucleus of a specimen gives rise to elastic scattering. All elements have unique spectral line energies and emit X-rays at their own characteristic lines. These spectral line energies are used for qualitative analysis, while their intensities for quantitative analysis. The X-rays emitted are named according to where the electron was emitted. For instance, if the X-rays are emitted by the electron filling the innermost shell (K-shell) then they are called "K-lines". For heavier elements, K lines require a huge amount of energy for an electron to be emitted. Hence, L and M lines are usually observed on the electron diffraction spectra (Yozana, 2015).

2.12.2. Energy Dispersive Spectroscopy (EDS)

EDS is an analytical technique used for the determination of elemental composition of a sample based on the interaction of some source of X-ray excitation with the sample. EDS is also used to stimulate the emission of characteristic X-rays from a specimen, using high energy beam of charged particles such as electros or protons (Atsile, 2012). The ground state electrons in electron shells bound to the sample in the nucleus get excited upon interaction by the incident beam. This often leads to ejection of electrons from the shell thus creating an electron hole. The number and energy of the X-rays emitted from a specimen can be using energy dispersive spectrometer. The X-rays has characteristic difference in energy between the two shells, and the atomic structure of the element from which they were emitted. This allows the elemental composition of the specimen to be measured (Goodge, 2013).

2.12.3. X-ray diffraction (XRD)

X-ray diffraction is a multidisciplinary analytical technique mostly used to obtain diffraction patterns of a sample via bombardment of such sample with X-rays to produce the mineralogical phase identity and crystal structure. X-rays are produced when fast moving electron in the wavelength range of 0.06 - 125 A° is slowed down in the electromagnetic radiation spectrum. Hence, X-rays are good probes for the determination of atomic arrangements of crystallographic materials due to their short wavelength (Suwarnkar *et al*., 2014). X-rays that are diffracted during XRD analysis provide information about the crystallinity of the sample, which may be single crystalline, polycrystalline, microcrystalline or amorphous in nature (Yozana, 2015).

2.12.4. Fourier Transform Infrared Spectroscopy (FT-IR)

Fourier-transform infrared spectroscopy is a technique used to obtain an infrared spectrum of absorption or emission of a solid, liquid or gas. The term TF-IR originates from the fact that a Fourier transform (a mathematical process) is required to convert the raw data into the actual spectrum. An FT-IR spectrometer simultaneously collects high-spectral-resolution data over a wide spectral range. This confers a significant advantage a dispersive spectrometer, which measures intensity over a narrow range of wavelengths at a time. The goal of FT-IR is to measure how much light a sample absorbs at each wavelength. The most way to do this is to shine a monochromatic light beam at a sample, measure how much the light is absorbed and repeat for various wavelengths. FT-IR relies on the fact that the most molecules absorb light in the infra-red region of the electromagnetic spectrum. The resultant absorption spectrum from the bond natural vibration frequencies indicates the presence of various chemical bonds and functional groups present in the sample.

2.12.5. Brunauer Emmett Teller (BET)

The BET theory was developed by Stephen Brunauer, Paul Emmett and Edward Teller in 1938. The first letter of each publisher's surname was taken to name this theory (BET). The BET theory was an extension of the Langmuir theory, developed by Irving Langmuir in 1916. The BET technique is used to study the pore size, pore volume, and surface area of a material. In BET surface analysis, nitrogen is usually used because of its availability in high purity and its strong interaction with most solids. Because the interaction between gaseous and solid phases is usually weak, the surface is cooled using liquid N_2 to obtain detectable amounts of adsorption. Known amounts of nitrogen gas are then released stepwisely into the sample cell. Relative pressures less than atmospheric pressure is achieved by creating conditions of partial vacuum (Yozana, 2015). After the saturation pressure, no more adsorption occurs regardless of any further increase in pressure. After the adsorption layers are formed, the sample is removed from the nitrogen atmosphere and heated to cause the adsorbed nitrogen to be released from the material and quantified. The data collected is displayed in the form of a BET isotherm, which plots the amount of gas adsorbed as a function of relative pressure and provide information on the surface area, pore volume and pore sizes of the sample.

CHAPTER THREE

3.0 MATERIALS AND METHODS

3.1 Sample Collection and Pretreatment

The fresh leaves of Azadiratcha Indica (Neem plant), were randomly collected from different locations in Bosso, Bosso Local Government Area, Niger Sate, Nigeria. The collected leaves were washed with water, cut into pieces, air dried for one week and then grounded with a wooden mortar and pestle. The powder was stored in an air tight container for subsequent uses.

The local dyeing wastewater was collected from Bida, Niger state. This sample was put in a gallon container and was and stored in the refrigerator at 4°C before analysis and usage.

3.2. List of Chemical Reagent and Equipment

Table 3.1 shows the list of chemical/reagents used in this work that were purchased from Sigma Aldrich and used without further purification while Table 3.2 represents the list of analytical equipments used for characterization of the synthesized nanoparticles.

Table 3.1: List of Chemicals

Chemical	Purity (%)	Supplier
Melamine	99.0	Sigma Aldrich
Sodium Hydroxide	97.0	Sigma Aldrich
Hydrochloric Acid	98.0	Sigma Aldrich

Table 3.2 List of Analytical Equipment

Equipment	Model	Location
SEM/EDS	Zeiss Auriga	University of Western Cape, South Africa
XRD	Bruker AxSD8 Cu-K radiation	Themba Laboratory Cape town, South Africa
BET	NOVA 2400e	STEP-B, FUTMINNA
FI-IR	Dw-Ftir-520A	Chemistry Department , University of Ilorin, Nigeria

3.3. Preparation of *Azadirachta Indica* aqueous leaves extract

Twenty grams (20 g) of the powdered leaves were weighed into a beaker containing 300 cm^3 of distilled water. This was boiled for 15 min at 60°C. The extract with the water was then allowed to cool at room temperature, filtered using Whatman No.1 filter paper. The obtained extract was poured into a bottle and stored in a refrigerator for further use.

3.4 Quantitative Determination of the Chemical Constituents in the Azadiratcha Indica leaves Extract.

3.4.1. Determination of Total Phenols

The total phenolic content was determined using Folin-Ciocalteau method as described by Cicco *et al*. (2009). Concentrations ranging from 0.2-1.0 mg/cm^3 of gallic acid and Azadiratcha Indica extracts were prepared in methanol. Thereafter, 4.5 cm^3 of distilled water was added to 0.5 cm^3 of the extract and mixed with 0.5 cm^3 of a ten-fold diluted Folin-Ciocalteau reagent. Five milliliters of 7.5 % sodium carbonate was then added to the tubes and another 2 cm^3 of distilled water was added. The mixture was allowed to stand for 90 min at room temperature and absorbance was then measured at 765 nm using shimadzu UV spectrophotometer (UV-1800, 240v). All determinations were performed in triplicates with gallic acid utilized as the positive control. The total phenolic content was expressed as Gallic Acid Equivalent (GAE).

3.4.2. Determination of Total Flavanoids

The total flavanoid content of the Azadirachta Indica methanol extract was determined according to Chang *et al*., (2002) method. 0.5 cm^3 of the extract was mixed with 1.5 cm^3 of methanol, 0.1 cm^3 of 1 M sodium acetate and 2.8 cm^3 of distilled water, and left to stand for 30 min. The absorbance of the reaction mixture was then measured at 415 nm using a double beam Shimadzu

UV-visible 1800 spectrophotometer. Quercetin was used as standard and a calibration curve was prepared. Total flavanoid was estimated using the equation (3.1).

$$Y = 1.2766x + 0.0448 \quad (3.1)$$

Where: Y is the absorbance (nm) and x is the concentration (mg/L).

3.4.3. Determination of Total Tannins

2.0 g of the powdered sample was measured into a 50 cm^3 beaker, followed by the addition of 20 cm^3 of 50 % methanol. The beaker was covered with foil paper and placed in a water bath at 77-80 °C for 1 h and thereafter shaken to ensure uniform mixing. The mixture was then filtered using the Whatman No.1 filter paper into a 100 cm^3 volumetric flask. 20 cm^3 of distilled water, 2.5 cm^3 of Folin-Denis solution and 10 cm^3 of 17 % Na_2CO_3 were added, mixed properly and allowed to stand for 20 min. The absorbance of the mixture was measured at 760 nm using Shemadzu UV- spectrophotometer (UV- 1800, 240v). Tannin was used as standard from tannic acid and a calibration curve was prepared. Total tannins were estimated using equation (3.2)

$$Y = 0.5269x + 0.602 \quad (3.2)$$

Where Y is the absorbance (nm) and x is the concentration (mg/L).

3.5 Synthesis of g-C_3N_4 nanoparticles

The g-C_3N_4 photocatalyst was prepared by the calcination of melamine powder in a closed system to prevent melamine sublimation. In detail, 10 g of melamine powder was placed in a ceramic crucible with a cover and then heated to 600 ^{O}C in a muffle furnace for 4 h at a heating rate of 4^{O} C/min. After natural cooling to room temperature, the obtained yellow agglomerate was ground into powder and used without further treatment.

3.6 Green Modification of the as-synthesized g-C_3N_4 Nanopartices

5 g of the synthesized g-C_3N_4 was added into a beaker containing 50 cm^3 of aqueous leaves extract of *Azadiratcha Indica*. The mixture was stirred continuously for 2 h in a magnetic stirrer. The resultant solution was allowed to age for 24 h after which it was oven dried at 80 °C for 7 h. The obtained sample was calcined at 500 °C for 2 h in a muffle furnace.

3.7. Characterization of the Prepared Catalysts

The modified and unmodified g-C_3N_4 samples synthesized were characterized using the following analytical techniques;

3.7.1 Scanning Electron Microscopy (SEM)

0.05 g of the synthesized samples was sprinkled on a carbon tape which was fixed onto an aluminium stub. The samples were coated with gold-palladium (Au:Pd; 60:40) using Quorum T15OT for 5 minutes prior to analysis. This was done to prevent charging which distort images during analysis. The Zeiss Auriga SEM coupled with EDS was used to examine the morphology and elemental composition of the samples. The microscope was operated at 5 KeV for imaging and 20 KeV detectors for EDS.

3.7.2. Energy Dispersive Spectroscopy (EDS)

0.05 mg of the synthesized materials sprinkled in a sample holder covered with carbon adhesive tape were sputter coated with Au-Pd using Quorum T15OT for 5 minutes prior to analysis. The sputter coated samples were characterized using Zeiss Auriga SEM. The secondary electron mode was activated for imaging and a homogeneous region on the sample was identified. The microscope was operated with electron high tension (EHT) of 20 KV for EDS, the illumination angle was adjusted to 150° and then the elemental composition of the sample was determined.

3.7.3 X-ray Diffraction (XRD)

1 g of the synthesized samples was crushed into powder and dispersed into a rectangular aluminium sample holder using a clean spatula. The sample holder containing the sample was clipped into the XRD instrument. Bruker AXS Advance diffractometer with 2θ range of 5 - 75°, a step size of 0.028°, and operating at 45 KV and 40 mA was used to collect the XRD data. Monochromatic copper (Cu) Kαl radiation with a wavelength of 0.154nm was as the X-ray source. The mean crystallite size of the nanoparticles (D), were obtained using the Debye-Scherrer's equation (Equation 3.3)

$$D = K\lambda/\beta\cos\theta \qquad 3.3$$

Where k is a Constance (k=0.94), λ = 1.54060 nm which is the Cu- Kαl wavelength, θ is the Bragg's angle and β is the full width half maximum (FWHM) of the peak at 2θ.

3.7.4. Textural Analysis

The analysis for the surface area, pore volume and pore size distribution of the samples was determined by Brunauer - Emmett- Teller (N_2 BET) technique using a NOVA 4200e surface area and pore analyzer instrument. Approximately 100 mg of the catalyst powder was weighed and degassed by flowing N_2 at 90 °C for 1 h, then held at 350 °C for 2 h. As the temperature is increased, water vapour was desorbed from the surface and pores of the sample. The sample was then cooled down and weighed again. The instrument uses physical adsorption and capillary condensation of N_2 principles to abstain information about the surface area and porosity of solid materials.

3.8. Blank and Control Experiment

3.8.1 Adsorption process

Prior to the photocatalytic activity studies, control experiments were conducted in the dark with the photocatalysts and local dyeing wastewater alone with continuous stirring for 6 h using magnetic stirring at 150 rpm. This was done in order to establish whether degradation of the organics in the dyeing wastewater was via adsorption technology and not photolysis or photocatalysis.

3.8.2 Photolysis experiment

In the photolysis experiment, 100 cm^3 of the local dyeing wastewater was exposed to sunlight alone for 6 h without catalyst. This was conducted to determine if the mineralization of the organics in the local dyeing wastewater at ambient temperature under sunlight irradiation without catalyst was due to photolysis and not adsorption or photocatalysis alone.

3.9 Photocatalytic experiment

The photocatalytic experiments of the modified and unmodified synthesized g-C_3N_4 were conducted in a batch reactor (500 cm^3 beaker). A known amount of the photocatalyst was placed in a reactor containing 200 cm^3 of real local dyeing wastewater and the solution pH was adjusted to 2, 4, 6, 8, 10 and 12. The mixture was then placed on a magnetic stirrer and stirred for 60 min in the dark before exposure to sunlight. This is to ensure that the adsorption-desorption equilibrium of the dye molecules on the catalyst surface had been reached. The whole set-up was then placed under sunlight with average intensity of 1.75 $\times 10^5$ Lux units or 252.92 W/m^2 at ambient temperature of about 35°C. The mixture was continuously stirred under sunlight irradiation and the process was monitored for 6 h. Sampling of 30 cm^3 aliquots was done from the batch set-up at various irradiation time intervals (0, 60, 120, 180, 240 and 300 min) and filtered using a Whatman (No.1) filter paper. The photocatalytic degradation of the local dyeing wastewater was then measured and the decrease in chemical oxygen demand COD as the

response parameter was evaluated. This procedure was repeated severally for each of the photocatalysts (modified and unmodified) with the pH adjusted in the range of 2-12 respectively. The photocatalytic activity was measured using the percentage of Chemical Oxygen Demand (COD) reduced after the photocatalytic experiment was conducted as shown in the equation (3.4)

$$\text{COD Removal (\%)} = [(C_O - C_f)/C_O] \times 100\% \qquad 3.4$$

Where Co is the initial COD of the wastewater and C is the COD remaining at a particular time in mg/L.

CHAPTER FOUR

4.0 RESULTS AND DISCUSSION

4.1 Phytochemical Screening of *Azadirachta indica* Leaves Extract

Table 4.1 shows the result of the quantitative phytochemical screening carried out on the aqueous leaves extract from *Azadirachta indica.*

Table 4.1 Phytochemical Assessment of the *Azadirachta indica* Leaves Extract

Content	Concentration (mg/ml)	Absorbance (nm)
Tannins	14.280	760
Phenols	1.620	765
Flavonoids	13.184	420

The phytochemical analysis was done in order to investigate the amount of tannins, phenols and flavonoids present in the leaves extract of the *Azadirachta indica*. It was discovered that the concentrations of tannins and flavonoids were higher than that of phenols, which suggests the suitability of the extract for modifying the g-C_3N_4 material. Similar findings were made by Vani *et al.* (2017). Studies have shown that these three phytochemical constituents are in most cases responsible for capping and stabilizing nanomaterials. This implies that these plants extracts behave in a similar manner with the commercial reducing agents such as citric acid, sodium borohydride ($NaBH_4$), lithium aluminium hydride ($LiAlH_4$). Phytochemical screening of the

methanolic extract showed the presence of flavonoids, phenols and tannins in different amounts similar to observation of Gomathi *et al*. (2012).

4.2. XRD Analysis

The XRD patterns of the modified and unmodified g-C_3N_4 was performed in the 2θ range of 5–75° using PAN alytical Bragg-Brentano diffractometer (radiation, λ= 1.5406 Å) and the results are shown in Figure 4.1. The modified and unmodified g-C_3N_4 prepared herein showed similar XRD patterns. The appearance of two peaks at value of 13.15° and 27.7° for both catalysts (modified and unmodified g-C_3N_4) are widely accepted as the g-C_3N_4 tri-s-triazine (Heptazine) building block. The peak indexed at 27.7° with a lattice plane of (0 0 2) indicates the characteristic stacking peak of aromatic compounds which is attributed to stacking of tri-s-triazine aromatic system where the electrons has stronger inter-layer binding. Similar observation was reported by Yang *et al*.(2013). The peak indexed at 13.15° corresponds to the lattice plane of (1 0 0), which also supports the stacking of tri-s-triazine aromatic electron system. For the modified g-C_3N_4 sample, the intensity of the peak of tri-s-triazine unit is much stronger than that of the unmodifiedg-C_3N_4. This essentially confirms the formation of richer electron density which will promote the formation of radicals leading to improved photoctalytic performance and regular stacking of C-N monolayers at (0 0 2) planar direction. The unmodified g-C_3N_4 sample showed lower intensity peak at (0 0 2) compared to the modified g-C_3N_4 sample as seen from the XRD result. This essentially indicates that modifying the graphitic carbon nitride enhances the crystallinity of the material.

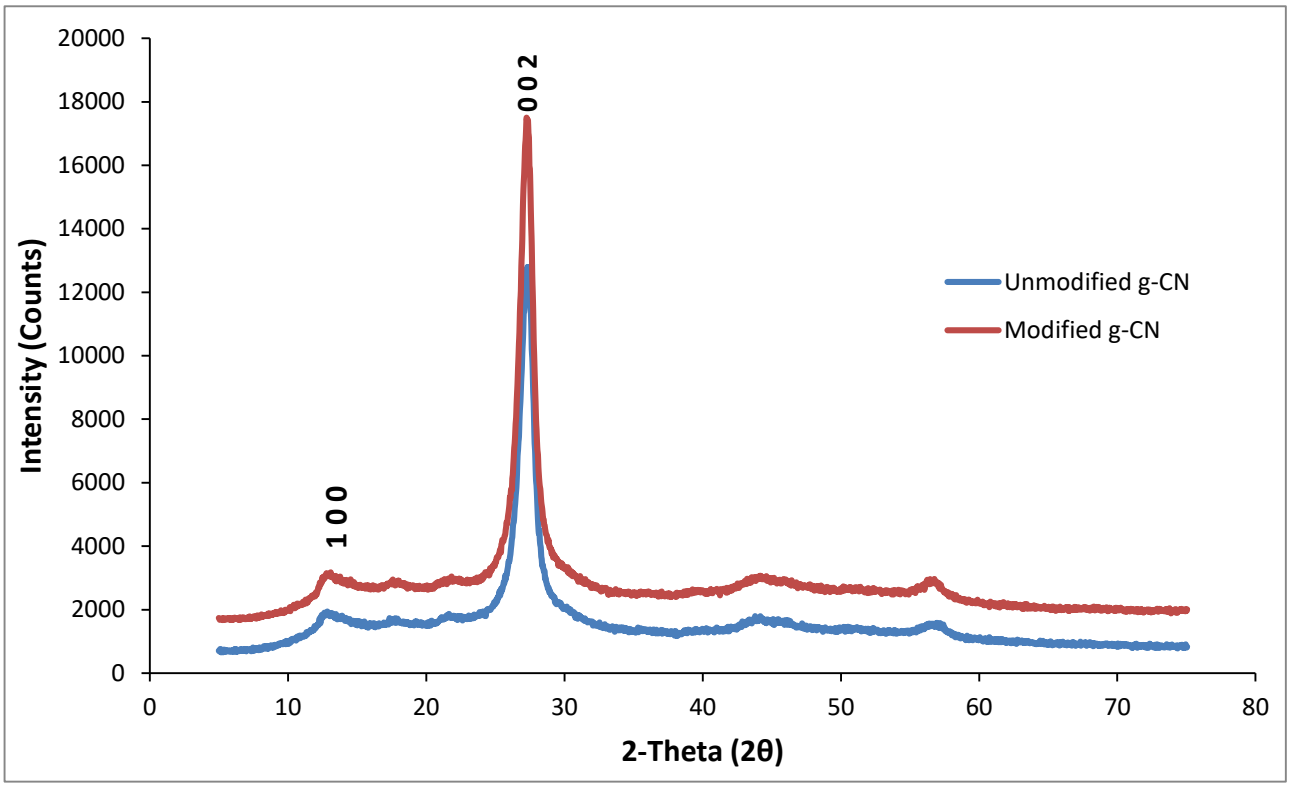

Figure 4.1: XRD Patterns of the Modified and Unmodified g-C_3N_4

4.3 SEM Analysis

It is clearly seen in Figure 4.2 (A-B) that the morphology of the modified g-C_3N_4 was smooth, thin and flat sheets with the formation of typical stacked lamellar layers of g-C_3N_4, while the unmodified g-C_3N_4 sample exhibits an aggregated (agglomerated) morphology. However, exhibition of less-agglomerated morphology by the modified g-C_3N_4 sample justifies its higher specific surface area. In addition, a typical porous morphology of g-C_3N_4 powder was also exhibited, which can be due to the presence of melem (heptazine or tri-s-triazine) units (Zhang *et al*., 2012). The morphologies of the g-C_3N_4 arrays in Figure 4.2 are in good agreement with the XRD result described in Figure 4.1.

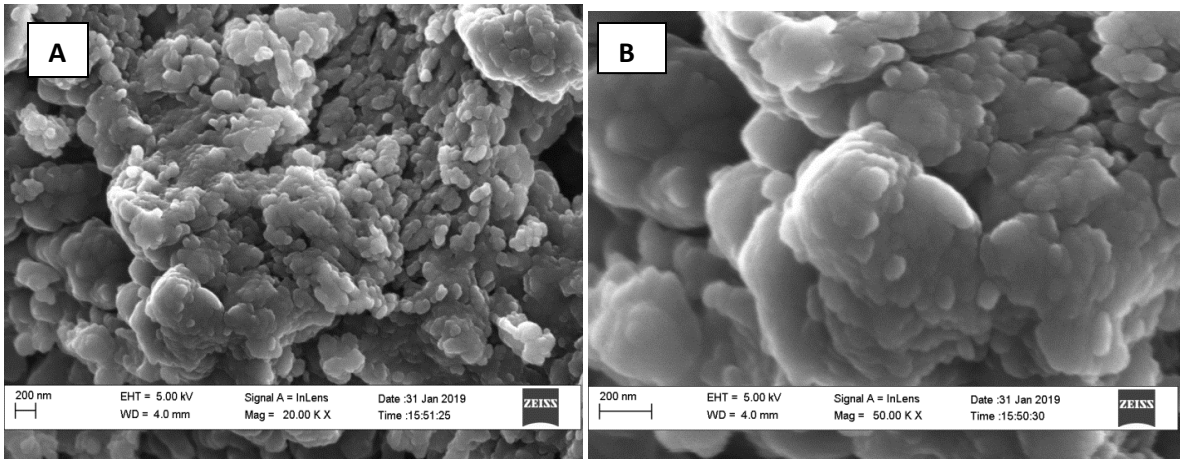

Fig.4.2: SEM micrograms of (A) Modified g-C_3N_4 and (B) Unmodified g-C_3N_4

4.4 EDS Analysis

The elemental composition of the modified and unmodified g-C_3N_4 was analysed using EDS. The EDS spectra showed only the presence of C and N as the dorminant elements, with a small amount of O. The origin of Oxygen is likely from the water (moisture) adsorbed on the surface of the samples during processing (Miller *et al*., 2017). Additionally, the EDS Mapping (appendix A) further demonstrates a successful fabrication of g-C_3N_4 nanoparticles.

Table 4.2: Elemental Composition of the Modified (M-g-C_3N_4) and Unmodified (U-g-C_3N_4) g-C_3N_4 Samples

Photocatalyst	C (Wt %)	N (Wt %)	O (Wt %)	Total (%)
M-g-C_3N_4	38.09	59.74	2.18	100
U-g-C_3N_4	36.33	61.67	1.99	100

4.5. Textural Analysis

The BET specific surface areas (Belsorp-MR6, MicrotracBEL) of the synthesized g-C_3N_4 have been analyzed from nitrogen adsorption and desorption isotherms by nitrogen multilayer adsorption measured as a function of relative pressure (P_s/P_0) in the range of 0.05–0.2. The summary of the BET results were tabulated and presented in Table 4.3. The BET analysis revealed that the modified sample (M-g-C_3N_4) exhibits mesoporous structure with a surface area of 141.0 m^2/g, while the unmodified sample (U-g-C_3N_4) showed a mesoporous structure with a comparatively lower surface area of 58.88 m^2/g. This could be attributed to the effects of the neem leaf extract which reduces the size of the particles; thus increases the total BET surface area. Also, the results showed that the modified graphitic carbon nitride (M-g-C_3N_4) has approximately 3 folds higher pore volume (0.08666 m^3/g) than the unmodified graphitic carbon nitride (0.03301 m^3/g). A similar improved surface area of 145.6 m^3/g was also obtained by Wang *et al*. (2018). The increased BET surface area of the modified g-C_3N_4 indicates that the separation and migration efficiency of the photogenerated carriers would be improved due to the creation of more surface active sites, so it can absorb and transfer reactant molecules easily via the interconnected porous structure which could consequently be in favor to the photocatalytic activity of the modified sample (Kong *et al*., 2017)

Table 4.3: The BET Specific Surface Area, Pore Volume and Pore Size of the Photocatalysts

Photocatalyst	BET Surface Area (m^2/g)	Pore Volume (cm^3/g)	Pore Size (nm)
U-g-C_3N_4	58.88	0.03301	2.128
M-g-C_3N_4	141.0	0.08666	2.132

4.6 FT-IR Analysis

The FT-IR spectra of the modified and unmodified g-C_3N_4 and samples showed similar characteristic vibrational peaks (Figure 4.3). A series of peaks found in the range from 1638–1246 cm^{-1} attributes to the typical stretching modes of C-N heterocycles. The sharp peak at 800 cm^{-1} is assigned to the bending vibration of tri-s-triazine rings, revealing that the structure of the obtained g-C_3N_4 is composed of *tri*-s-triazine units. Similar findings were made by Lan *et al*. (2017). The diffraction peak at 800 cm^{-1} and 1638–1246 cm^{-1} for the modified g-C_3N_4 suggests the tri-s-triazine units with more ordered in-plane structural packing motif (Liang *et al*., 2015). The broader absorption band located at 3285 cm^{-1} originated from the stretching vibration of N-H bonds associated with amino and OH groups. The enhanced absorption in 3285 cm^{-1} can be considered as an indicator of modified g-C_3N_4 with enlarged open-up surfaces and amino groups (Cui *et al*., 2016).

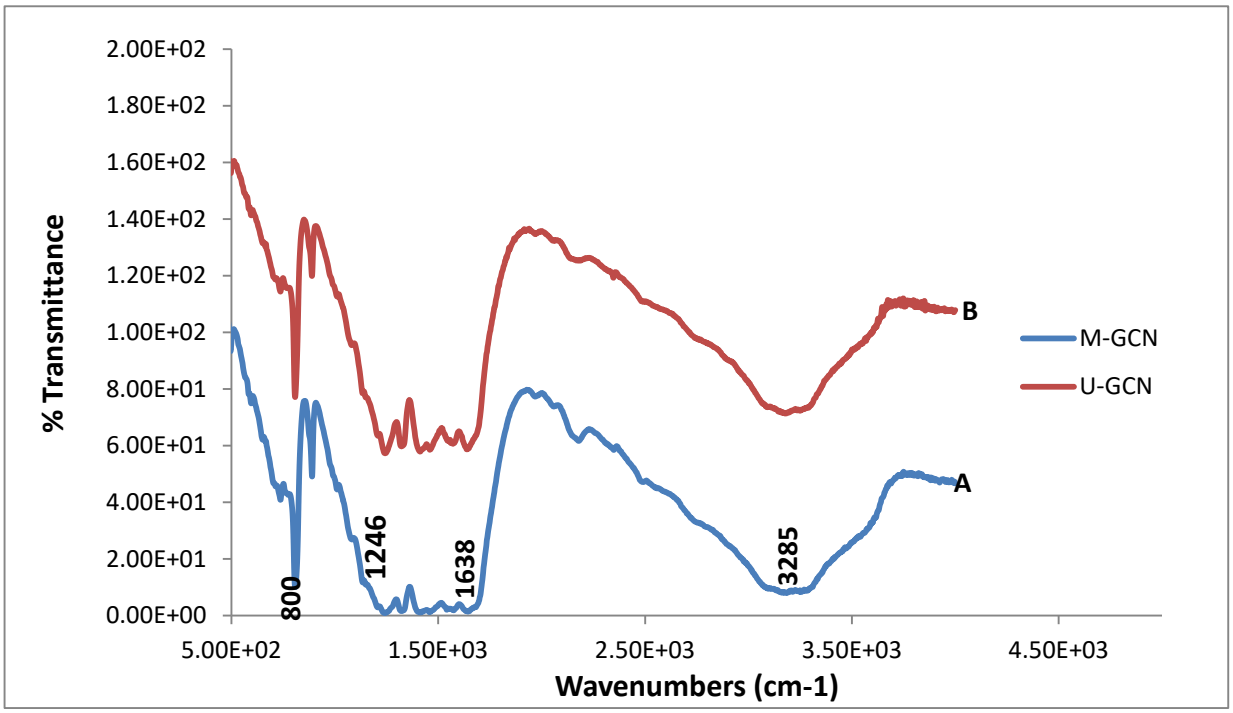

Figure 4.3: FT-IR Spectra (A) Modified Graphitic Nitride (M-GCN) and (B) Unmodified Graphitic Carbon Nitride (U-GCN)

4.7 Effects of Experimental Conditions on the COD Reduction Process

The photocatalytic activities of the s modified and unmodified g-C_3N_4 were investigated by the degradation of organic pollutants in real dyeing wastewater under sunlight irradiation. The oxidative mineralization of the organic pollutants in the dyeing wastewater by the photocatalysts was measured using COD as indicator parameter. Moreover, prior to the oxidative degradation experiment, blank experiments involving the use of light alone (photolysis) or catalyst alone in the dark (adsorption) were carried out to confirm the COD reduction is due to oxidation process and not by the photolysis or adsorption process. It was observed that COD concentration did not change when light or catalyst alone was used. This signifies that COD reduction did not follow photolysis or adsorption process.

4.7.1 Effect of photocatalyst loading

In order to investigate the effect of photocatalyst dosage on the degradation process, experiments were conducted with different photocatalyst loading in the range of 0.1 g - 1 g in 200 ml of the wastewater sample at default solution pH of 10.4 with a total treatment time of 6 hrs under solar irradiation. The results are depicted in Figure 4.4. The results revealed that the rate of degradation was increased with the photocatalyst loading in the reaction solution. When the catalyst dosage was increased from 0.1g to 1g, the COD reduction was increased from 33% to 39 % under solar irradiation. However, the highest (optimum) reduction efficiency was obtained with 0.7 g photocatalyst loading. This optimum photocatalyst dosage was in good agreement with the findings of Alseroury, (2018) who obtained an optimum dosage of 0.75g. But, reduced degradation efficiency was observed when the photocatalyst loading was increased from 0.7 g to 1.0 g (figure 4.4). This could be attributed to the fact that increasing the photocatalyst loading into the reaction solution increased the number of •OH radical production by facilitating more surfaces where radicals are generated. But, at higher concentration of photocatalyst, the degradation efficiency was decreased due to low penetrability of sunlight through the reaction solution (Pang *et al*., 2010). Hence screening effect due to the high concentration of photocatalyst in the reaction solution bound the electron excitation during photocatalysis oxidation process, thereby reducing the degradation efficiency to a certain level. In addition, for a catalyst in suspension, agglomeration may occur at higher concentrations, which reduces the available active sites along with a resulting decrease in efficiency (Huang and Shu, 2017).

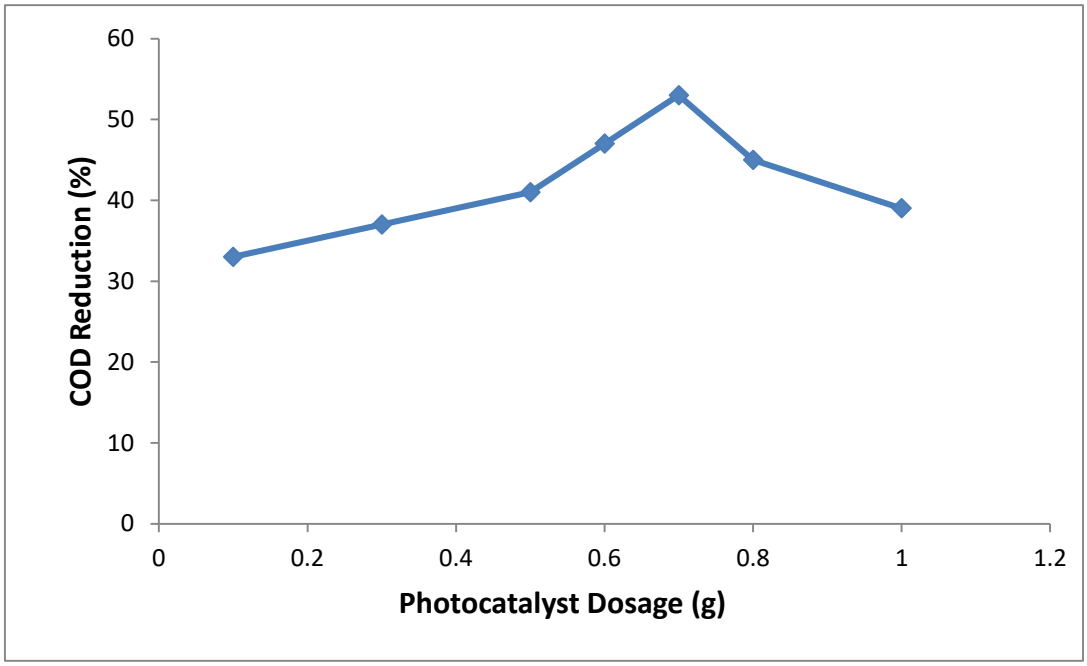

Figure 4.4: Effect of Photocatalyst Loading on COD Reduction

4.7.2 Effect of solution pH

The pH of the medium has direct influence in degradation process of organic pollutant from wastewater irrespective of treatment type whether it is physical, chemical or biological process. Therefore, the initial solution pH is considered to be a key operating parameter which influences the degradation efficiency or rate constant of any chemical reaction. It has significant effect on the efficiency of organic pollutant removal, activity of the oxidants used during treatment, properties of the catalyst and activities of the reactive species (Rahmani *et al*., 2012). Hence, in other to investigate the effect of solution pH on COD reduction efficiency, batch experiments were conducted with constant optimum photocatalyst dosage of 0.7g at different pH (2 - 12) and the results are presented in Figure 4.5. From the experimental results, it was observed that COD reduction efficiency is not significant in acidic conditions. On the other hand, the reduction efficiency was increased in alkaline condition up to 9.8 (optimum) with a maximum degradation efficiency of 61% achieved under solar irradiation. The increased COD reduction efficiency under alkaline condition could be attributed to the pronounced presence of the highly oxidative

•OH radical whose production is favoured in alkaline medium (Alvarez *et al*., 2016). Hence, the overall photocatalytic degradation of dyeing wastewater was significantly enhanced. In addition, positive holes are the predominant oxidation species at low pH while •OH are abundant in wastewater at high and neutral pH (Akpan and Hameed, 2009). This implies that degradation would be enhanced in alkaline wastewater because coulombic repulsion with hydroxide anions would not be present.

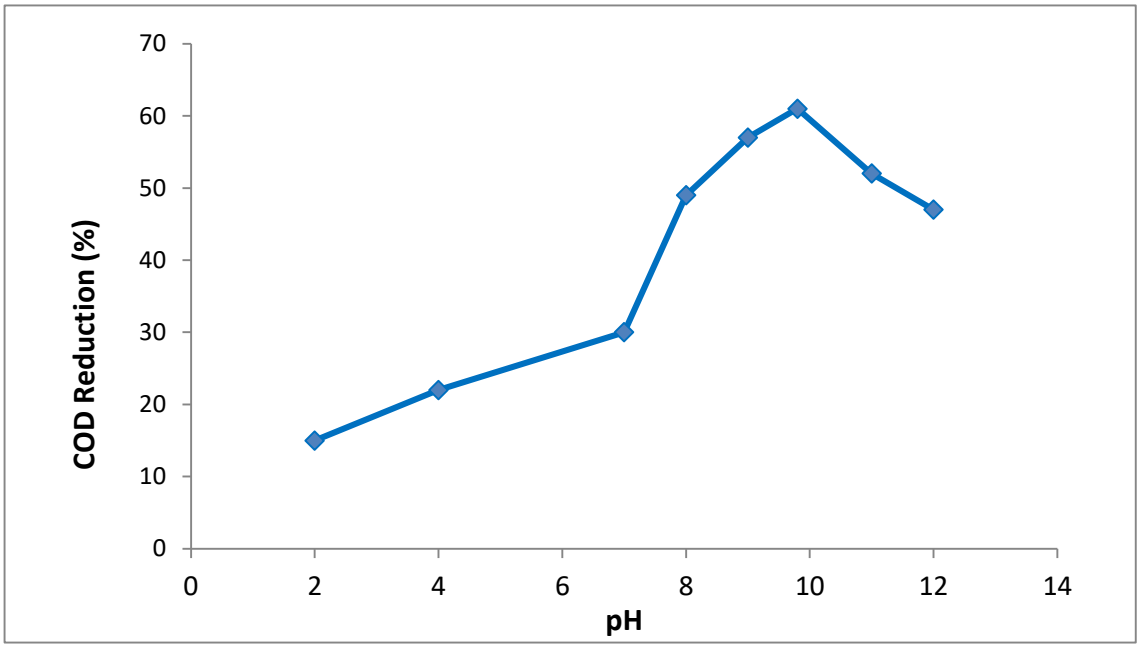

Figure 4.5: Effect of Solution pH on the COD Reduction

4.7.3. Effect of Reaction Time

The impact of time on the photocatalytic activity of the modified and unmodified g-C_3N_4 samples were investigated via the degradation of local dyeing wastewater under sunlight irradiation for the period of 6 h. The percentage reduction of COD as the indicator parameter and the kinetics of the reaction were evaluated using first order, second order and Behnjady-Modirshahla- Ghanbery (BMG) models. A linear relationship was observed between irradiation

time and COD reduction. It was also observed from the result as presented in Figure 4.6 that the modified g-C_3N_4 showed higher COD reduction of 61% as compared to the unmodified g-C_3N_4 which showed 41% COD reduction under 6 h irradiation time. The observed higher catalytic efficiency of the modified g-C_3N_4 may be linked to its higher surface area of 141 m^2/g which was 2.4 times greater than the surface area of the unmodified g-C_3N_4.

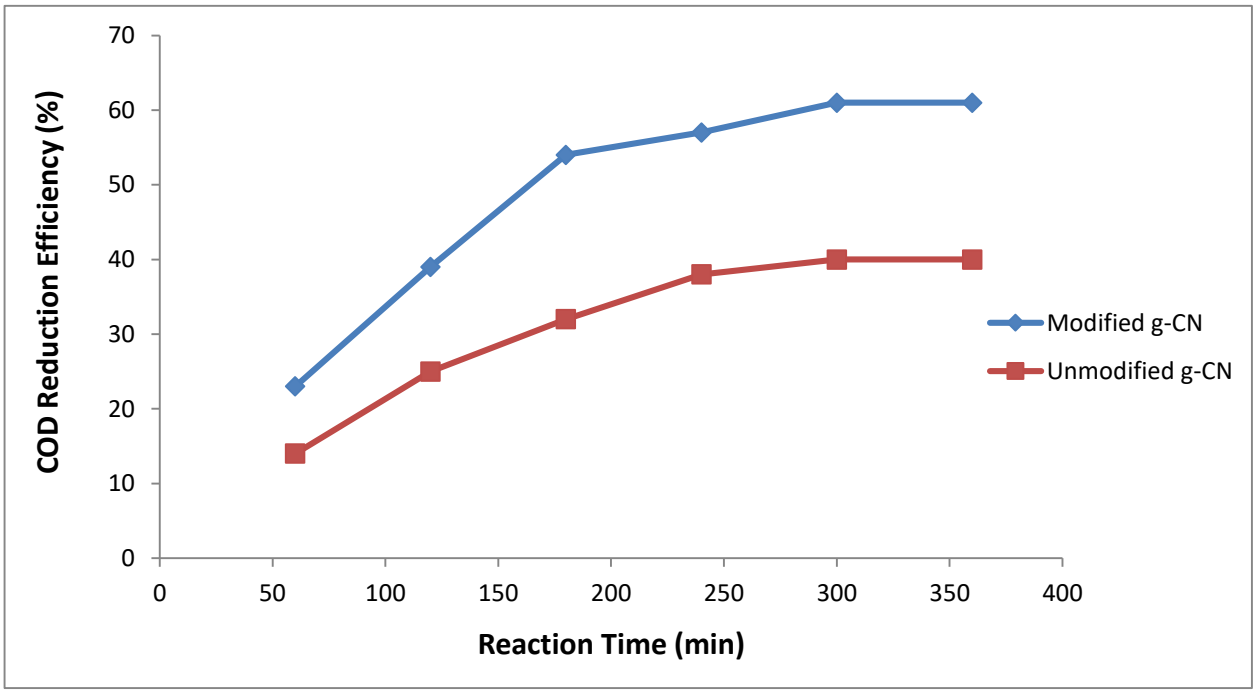

Figure 4.6: Effect of Time on the COD Reduction

4.8 Kinetics Studies for the Photodegradation of Organics in Local Dyeing Wastewater by the Modified g-C_3N_4 Nanoparticles.

In the present study, first-order, second-order and BMG reaction kinetics were used to study the COD reduction kinetics of the dyeing wastewater by the photocatalysts. The kinetic data obtained from COD reduction at different time were fitted into the three models and the result of the apparent rate constant (K) and correlation coefficient (R^2) of each photocatalyst with respect to the dyeing wastewater is presented in Table 4.4. The photocatalysts demonstrated a linear relationship between the amount of COD reduced and irradiation time (Appendices B & C). It can be seen from Table 4.4 that the rate constant (K) for the unmodified g-C_3N_4 for the first order model is 0.0014 min^{-1}, which however increased from 0.0014 min^{-1} to 0.0029 min^{-1} for the modified g-C_3N_4. Similar trend was observed for the second order Model. The values of correlation coefficient (R^2) and the apparent rate constants values (K) for BMG model are mostly higher than those of the first-order and the second-order models. The calculated regression coefficients (R^2) of the BMG kinetic model were 0.9832 and 0.9823 respectively for the modified and unmodified g-C_3N_4.This signifies faster reduction of COD by the reactive species (•OH, •O_2) generated by the g-C_3N_4 into harmless compounds such as CO_2 and H_2O. Therefore, BMG kinetic model is the best model to describe the photocatalytic degradation of organic pollutants by neem leaf extract modified g-C_3N_4 photocatalyst.

Table 4.4: The Parameters of Kinetic Models and Correlation Coefficients (R^2) for the COD Reduction of Local Dyeing Wastewater by g-C_3N_4 Nanoparticle

Kinetic Model		Photocatalyst	
		Modified g-C_3N_4	**Unmodified g-C_3N_4**
First order	R^2	0.9343	0.9802
	K (min^{-1})	0.0029	0.0014
Second order	R^2	0.9617	0.9802
	K ($Lmg^{-1}min^{-1}$)	$2x10^{-5}$	$9x10^{-6}$
BMG	R^2	0.9832	0.9823
	1/b	0.9752	0.7071
	1/m	0.0057	0.0031

CHAPTER FIVE

5.0 CONCLUSIONS AND RECOMMENDATIONS

5.1 Conclusions

The photocatalytic COD reduction in real local dyeing wastewater could be achieved using neem-modified graphitic carbon nitride nanoparticles under sunlight irradiation. The research objectives were successfully achieved with the outcome of the findings as summarized:

The XRD and SEM characterizations revealed a crystalline and agglomerated lamellar morphology of the photocatalysts, while the EDS analysis demonstrated the presence of C and N as the only constituents. The BET surface area of the modified g-C_3N_4 exhibited a mesoporous structure with 141.0 m^2/g, which is 2.4 times higher than the surface area of the unmodified g-C_3N_4 (58.88 m^2/g).

The modified g-C_3N_4 achieved better COD reduction of 61 % in comparison to the unmodified g-C_3N_4 which showed 40 % COD reduction under 6 h sunlight irradiation time. The enhancement in performance is because of its improved surface area which signifies more active sites for reaction, small bulk diffusion length and strong redox ability of charge carriers. It was established from the optimization study that pH of 9.8 and photocatalyst dosage of 0.7 g/200 ml were the optimum conditions. The adsorption, photolysis and photodegradation results revealed that the degradation is mainly due to photocatalysis.

The BMG kinetic model best fits the kinetic data in comparison to the first order and second order models based on the value of correlation coefficient obtained. The adsorption, photolysis and photodegradation results revealed that the degradation is mainly due to the oxidation process. This finding is fascinating in encouraging researchers to test their as-developed

photocatalyst using real industrial wastewater instead of synthetic or mimicking wastewater.

5.2 Recommendations

Sequel to the findings of this study, a few recommendations were made regarding future research as follows:

i. Other parameters such as the effects of optimum volume/mass mixing ratio of the neem leaf solution and g-C_3N_4 and the calcination temperature on the modified g-C_3N_4 nanoparticles should be investigated.

ii. Future research on photocatalytic degradation of organics should focus on the effects of variations of; light intensity, temperature, volume of the wastewater on the performance of the as-synthesized g-C_3N_4 photocatalyst.

iii. The results of this finding demonstrated that organic pollutants in dyeing wastewater can be degraded into environmentally friendly by-products using g-C_3N_4 photocatalyst under sunlight irradiation. However, the activities of the photocatalyst on other industrial wastewaters such as pharmaceutical, tannery, poultry, brewery and petroleum, need to be examined.

iv. Studies on the reusability of the modified g-C_3N_4 photocatalyst should be conducted.

v. Apart from its role as a metal-free photocatalyst, it is also important to seek for new applications of g-C_3N_4 in catalysis.

REFERENCES

Ai, B., Duan, X.G., Sun, H.Q., Qiu, X., & Wang, S.B. (2015). Synthesis of graphene-carbon nitride hybrids by the method of thermal condensation of melamine and GO, *Catalysis Today journal*, 258, 668-675.

Akpan, U.G., & Hameed, B.H. (2009). Parameters affecting the photocatalytic degradation of dyes using TiO_2-based photocatalysts: a review. *Journal of hazardous materials*, 170(2-3), 520-529.

Akpan, U.G., & Hameed, B.H. (2010). The advancements in Sol-gel method of doped-TiO_2 photocatalysts, *International journal of Applied Catalysis A*, 375(1), 1-11.

Akple, M.S., Low, J.X., Wageh, S., Al-Ghamdi, A.A., Yu, J.G., & Zhang, J. (2015). Modification of g-C_3N_4 with metal sulfides for enhanced photocatalysis, *Journal of Applied Surface Science*, 358, 196-203

Alivisatos, A. P. (1996). Semiconductor Clusters, Nanocrystals, and Quantum Dots. *Science Direct*, 271, 933−937.

Alseroury, F.A. (2018). Solar light assisted catalysis process with g-C_3N_4Nanomaterialsto improve biological treatment of cheese whey wastewater. *International Journal of Pharmaceutical and Phytopharmacological Research*. 8(5), 12-19

Álvarez, M.A., Rivera-Utrilla, J., Sánchez-Polo, M., López-Ramón, M.V., & Orellana-García, F. (2016). Influence of operational parameters on photocatalytic amitrole degradation using nickel organic xerogel under UV irradiation. *Arabian Journal of Chemistry*. 11, 564–572.

An, C.H., Peng, S.N., & Sun, Y.G. (2010). Synthesis of AgCl:Ag plasmonic nanoparticles as photocatalysts for efficient degradation of organics under sunlight. *Journal of AdvancedMaterials*, 22, 2570-2574.

Anpo, M.,T Kim, T.H., & Matsuoka, M. (2009). Synthesis and photocatalytic activity of Ti-, V-, Cr-oxide single-site photocatalysts. International *journal of Catalysis today*, 142, 114-124.

Ansari, S.A., Ansari, M,O., & Cho, M.H., (2016). The feasible synthesis of g-C_3N_4/red phosphorus and its potential applications for degradation of dyes and energy storage. *ScientificReports journal*, 6, ARTN27713.

Arshad, H., Shadma, W., Iffat, Z., & Sarfaraj, H. (2010). Antibacterial activity of the leaves of Coccinia indica. *Advanced Biological Research*, 4, 241-248.

Asahi, R., Morikawa, T., Ohwaki, T., Aoki, K., & Taga, Y. (2001). Synthesis of nitrogen-doped TiO2 and its application in visible light photocatalysis. *Science Journal*, 293, 269-271.

Asapu, R., Palla, V.M., Wang, B., Guo, Z.H., Sadu, R., & Chen, D.H. (2011). Synthesis of phosphorus visible-light-driven TiO_2 photocatalysts. *Journal of Photochemistry and Photobiology A*, 225, 81-87.

Bai, X.J., Wang, L., Zong, R.L., & Zhu, Y.F., (2013). Transformation of g-C_3N_4 nanorods from nanoplates by a simple reflux method. *Journal of Physical Chemistry C*, 117, 9952-9961.

Bao, N.Z., Shen, L.M., Takata, T., & Domen, K. (2008). Development of CdS for visible light catalysis. *Journal of chemical Materials*, 20, 110-117.

Baruah, S., Khan, M.N., & Dutta, J., (2015). Perspectives and applications of nanotechnology in water treatment. Environmental chemistry letter, 14, 1-14.

Basu, M., Sinha, A.K., Pradhan, M., Sarkar, S., Negishi, Y., & Pal, T. (2010). Photodegradation activity of CuS on organic pollutants in water. *Journal of Environmwntal Science and Technology*, 44, 6313-6318.

Benelli, G., Govindarajan, M., Kadaikunnan, S., & Alharbi, N.S. (2017) what kind of reducing botanical? High mosquitocidal efficacy of a silver nanocomposite synthesized using a leaf aqueous extract ofFumaria indica. *Journal of Cluster Science*. 28, 637–643.

Bhatkhande, D.S., Pangarkar, V.G., & Beenackers, .A.C., (2002). Photocatalytic degradation for environmental applications–A review. *Journal of Chemical Technology & Biotechnology*, 77 (1). 102–116.

Bhattacharyya, K.G., & Sarma, A., (2003). Adsorption characteristics of the dye, Brilliant Green, on Neem leaf powder. *International Journal of Dyes and Pigments*, 57 (3). 211–222.

Blake, D. (2001). Bibliography of work on the heterogeneous photocatalytic removal of hazardous compounds from water and air – Update Number 4 to October 2001.

Borase, H.P., Bipinchandra, K., Salunke, R.B., Salunkhe, C., Patil, D., John, E., Hallsworth, B., Kim, S., & Patil, S.V. (2014). Plant extract: a promising biomatrix for ecofriendly, controlled synthesis of silver nanoparti-cles. Applied Biochemistry and Biotechnology. 173,1–29.

Bussi, J., Ohanian, M., Vázquez, M., & Dalchiele, E.A. (2002). Photocatalytic removal of Hg from solid wastes of chlor-alkali plant. *Journal of Environmental Engineering* 128 (8). 733–739.

Cantrella, M., Sanz, R., Buccheri, M.A., Romano, L., & Privitea, V. (2015). PMMA/TiO_2 nanaotubes composites forphotocatalytic removal of organic coumpounds and bacteria from water. *Journal of science in semiconductor processing*, 42(1), 58-61.

Cao, S., Low, J., Yu, J., & Jaroniec, M. (2015). Polymeric photocatalysts based on graphitic carbon nitride. *Journal of Advanced Materials* 27, 2150–2176.

Chang, C., Yang, M., Wen, H., & Chern, H. (2002). Estimation of total flavanoid content in propolis by two complementary calorimetric methods. Journal of food and drug analysis, 10, 178-182.

Chen, D.M., Jiang, Z.Y., Geng, J.Q., Wang, Q., & Yang, D. (2007). Co-doping studies of graphitic carbon nitride with other elements. *Journal of Industrial and Engineering Chemistry Research*, 46, 2741-2746.

Chen, J.B., Che, H.N., Huang, K., Liu, C.B., & Shi, W.D. (2016). The applications of plasmonic photocatalysis for degradation, hydrogen production, and chemical synthesis. *Journal of Applied Catalysis B-Environmental*, 192, 134-144.

Chen, S.F., Hu, Y.F., Meng, S.G., & Fu, X.L., (2014). Modification of g-C_3N_4 with WO_3 for enhanced photocatalysis, *Journal of Applied Catalysis B-Environmen*t, 150, 564-573.

Chen, X., Zhu, H.Y., Zhao, J.C., Zheng, Z.T., & Gao, X.P. (2005). Synthesis and photodegradation of gas pollutants under sunlight by metal oxide-supported Au nanoparticles. *Angewandte Chemie International Edition*, 47, 5353-5356.

Cho,Y.M., Choi, W.Y., Lee, C., Hyeon, T., & Lee, H.I. (2001). Dyes as effective sensitizers to harvest visible light for photocatalysis. *Journal of Environmental Science and Technology*, 35, 966-970.

Chong, M.N., Jin, B., Chow, C.W., & Saint, C. (2010). Recent developments in photocatalytic water treatment technology: A review. *Journal of Water Research*, 44 (10), 2997–3027.

Chu, S., Wang, W., Guo, Y., Feng, J., Wang,C., Luo, W., Fan, X., & Zou, Z. (2013). Band structure engineering of carbon nitride: in search of a polymer photocatalyst with high photooxidation property. *Journal of American Chemical Society*, 3, 912–919.

Cicco, N., Lanorte, M., Paragio, M., Viggiano M., & Lattanzio, V. (2009). A reproducible, rapid and inexpensive Forlim-Ciocalteu micro method in determining phenolics of plant methanol extracts. *Michrochemical journal*, 91(1), 107-110.

Cui, J., Liang, S.H., Wang, X.H., & Zhang, J.M. (2015). Investigation of the effect of oxygen doping on the electronic and geometric structure of g-C_3N_4 by the first principle. *Materials Chemistry and Physics journal*, 161, 194-200.

Cui, Y., Zhang, G., Lin, Z., & Wang, X. (2016). Condensed and low-defected graphitic carbon nitride with enhanced photocatalytic hydrogen evolution under visible light irradiation. *Applied Catalysis B: Environmental*. 181, 413–419. https://doi.org/10.1016/j.apcatb.2015.08.018

Dariani, R.S., Esmaeili, A., Mortezacli, A., & Dehghanpour, S. (2016). Photocatalytic reaction and degradation of methylene blue on TiO_2 nano-sized particles. *Journal Optik*, 127, 7143-7154.

Das, R. (2014). Application of photocatalysis for treatment of industrial wastewater- a review. *Open access library journal*, 1:e713. http://dx.doi.org/10.4236/oalib.1100713.

Deepa, M.K., Suryaprakash, T.N., & Pawan, K. (2016). Green synthesized silver nanoparticles. *Journal of chemical and pharmaceutical research*, 8(1), 411-419.

Dong, X.P., & Cheng, F.X. (2015). The exfoliation strategies for synthesis of two-dimensional g-C_3N_4 nanosheets, *Journal of Materials Chemistry* A, 3, 23642-23652.

Fang, J., Fan, H., Zhu, Z., Bing, L., & Ma, L. (2016a). Dyed graphitic carbon nitride with greatly extended visible-light-responsive range for hydrogen evolution. *Journal of Catalysis*, 339, 93–101.

Fang, J.W., Fan, H.Q., Zhu, Z.Y., Kong, L.B., & Ma, L.T. (2016b). Effects of the pre-treatment of carbon nitride precursor on the g-C_3N_4 samples. *Journal of Catalysis*, 339, 93-101.

Faust, B.C., Hoffmann, M.R., & Bahnemann, D.W. (1989). α-Fe_2O_3 as an efficient photocatalyst for photocatalytic oxidation of SO_2 in water. *Journal of Physical Chemistry*, 93, 6371- 6381.

Gao, J.K., Miao, J.W., Li, P.Z., Teng,W.Y., Yang, L., Zhao, Y.L., Liu, B., & Zhang, Q.C. (2014). Development of metal-organic frameworks (MOFs) photocatalysts. *Journal of Chemical Communications*, 50, 3786-3788.

Gao, Q.S., Giordano, C., & Antonietti, M. (2011). TaON as an effective visible light photocatalyst for water splitting. *Small*, 7, 3334-3340.

Gaya, U.I., & Abdullah, A.H., 2008. Heterogeneous photocatalytic degradation of organic contaminants over titanium dioxide: A review of fundamentals, progress and problems. *Journal of Photochemistry and Photobiology C*, 9 (1), 1–12.

Ghaly, A.E., Ananthashankar, R., Alhattab, M., & Ramakrishman, V.V. (2014). Production, characterization and treatment of textile effluents. *Journal of chemical engineering process technology*, 5(8), 182-187.

Gomathi, P., Guptha, M., & Mazumder, U.K. (2012). Chronic toxicity studies of plumeria acuminate and Galega purpurea in experimental animals. *International journal of experimental sciences and research*, 3(7), 2017-2112.

Goodge, J. (2013). Integrating research and education: Techniques X-ray power Diffraction, http:///www.MSDS and intstrumentation/EDS.html.

Groenewolt, M., & Antonietti, M. (2005). physicochemical properties of graphitic carbon nitride. *Journal of Advanced Materials*, 17, 1789-1792.

Guan, L., Xu, N., Liu, X., Zhao, Y., Li, H., Sun, J., Wu, J., & Ying, Z. (2014). Controlled growth of crystalline g-C_3N_4 nanocone arrays by plasma sputtering reaction deposition. *Carbon*, S0008-6223(14)00759-3, doi: http:// dx.doi.org/10.1016/j.carbon.2014.08.019.

Guo, H.X., Ke, Y.C., Wang, D.F., Lin, K.L., Shen, R.X., Chen, J.H., & Weng, W. (2013). Photodegradation activity of NiS on organic pollutants in water. *Journal of Nanoparticles Research,* 15, ATN 1475.

Guo, Q. X., Xie, Y., Wang, X. J., Lv, S. C., Hou, T., & Liu, X. M. (2003). Characterization of Well-Crystallized Graphitic Carbon Nitride Nanocrystallites via a Benzene-Thermal Route at Low Temperatures. Chemical Physics Letters, 380 (1–2), 84–87. doi:10.1016/j.cplett.2003.09.009.

Guo, S.E., Deng, Z.P., Li, M.X., Jiang, B.J., Tian, C.J., Pan, Q.J., & Fu, H.G. (2016). Synthesis of holey-structured g-C_3N_4 with doped oxygen at the edges via photo-Fenton reactions. *Angewandte Chemie International Edition*, 55, 1830-1834.

Guo, W., Qin, Q., Geng, L., Wang, D., Guo, Y.H., & Yang, Y.X. (2016). Synthesis of P-doped carbon nitride tubes using hexagonal rod-like supramolecular as the precursor of g-C_3N_4 and phosphorous acid as a P source and its application to hydrogen evolution reactions. *Journal of Hazardous Materials*, 308, 374-385.

Gupta, V.K., Ali, I., Saleh, T.A., Nayak, A., & Agarwal, S. (2015). Chemical treatment technologies for waste-water recycling – An overview. *Royal Society of Chemistry Advances*, 2 (16), 6380–6388.

Gupta, V.K., & Suhas. (2013). Application of low-cost adsorbents for dye removal – A review. *Journal of Environmental Management*, 90 (8), 2313–2342.

Hadi, H.M., & Wahab, H.S. (2015). Visible light photocatalytic decolourization of methyl orange using N-Doped TiO_2 nanoparticle. *Journal of Al-Nahrain University*, 18(3), 1-9.

Han, Q., Wang, B., Gao, J.,Z., Cheng, Z.H., Zhao, Y., Zhang, Z.P., & Qu, L.T. (2016). Synthesis of mesoporous g-C_3N_4 nanomesh by solvothermal exfoliation. American Chemical Society *Nano- journal*, 10, 2745-2751.

Harikumar, P.S., Joseph, L., & Dhanya, A. (2013). Photocatalytic degradation of textile dyes by hydrogen supported titanium dioxide nanoparticles. *Journal of environmental engineering and ecological science*, 3(2), 123-129.

He, F., Chen, G., Yu, Y.; Hao, S., Zhou, Y., & Zheng, Y. (2014). Facile Approach to Synthesize g-PAN/g-C_3N_4 Composites with Enhanced Photocatalytic H_2 Evolution Activity. *Journal of Applied Materials Interfaces*, 6, 7171−7179.

He, Y., Zhang, L., Teng, B., & Fan, M. (2015). New application of z-scheme Ag_3PO_4/g-C_3N_4 composite in converting CO_2 to fuel. *Jounal of Environmental Science Technology*, 49, 649–656.

Hisatomi, T., Teramura, K., Kubota, J., & Domen, K. (2014). $Zn_xTiO_yN_z$ as an effective visible light photocatalyst for water splitting. *Bulletine of the Chemical Society of Japan*, 81, 1647-1656.

Hitoki, G., Ishikawa, A., Takata, T., Kondo, J.N., Hara, M., & Domen, K. (2002). Ta_3N_5 as an efficient photocatalyst responding to visible light and producing hydrogen and oxygen from water splitting. *Chemistry Letters journal*, 736, 736-737. DOI: 10.1246/cl.2002.

Holkar, C.R., Jadhav, A.J., Pinjari, D.V., Mahamuni, N.M., & Pandit, A.B., (2016). A critical review on textile wastewater treatments: Possible approaches. *Journal of Environmental Management*, 182, 351–366.

Hong, J.D., Xia, X.Y., Wang, Y.S., & Xu, R. (2012). Synthesis of mesoporous g-C_3N_4 with SiO_2 nanoparticles as the hard template. *Journal of Materials Chemistry*, 22, 15006-15012.

Hou, Y.D., Wang, X.C., Wu, L., Ding, Z.X., & Fu, X.Y. (2006). β-Ga_2O_3 for efficient photodegradation of gaseous benzene in air under UV ligh. *Journal of Environmental Science Technology*, 40, 5799-5803.

Hu, A. (2013). Enhanced photocatalytic degradation of Dyes by TiO_2 Nanaobelts with Hierarchial Structures. *Journal of photochemistry and photobiology A: Chemistry*, 256, 7-15.

Hu, J.S., Ren, L.L., Guo, Y.G., Liang, H.P., Cao, A.M., Wan, L.J., & Bai, C.L. (2005). Synthesis of ZnS nanoparticle for hydrogen production and CO_2 conversion. *Angewandte Chemie International Edition*, 44, 1269-1273.

Huang, C.R., & Shu, H.Y. (2017). The reaction kinetics, decomposition pathways and intermediate formations of phenol in ozonation, UV/O_3, and UV/H_2O_2 processes. *Journal of Hazardous Materials*. 41, 47–64.

Huang, Z.A., Sun, Q., Lv, K.L., Zhang, Z.H., Li, M., & Li, B. (2015). Synthesis of O-doped g-C_3N_4 by a precursor pre-treatment method. *Journal of Applied Catalysis B-Environment*, 164, 420-427.

Huang, Z.J., Li, F.B., Chen, B.F., & Yuan, G.O. (2016). Synthesis of Openly-structured microspheres of g-C_3N_4 with an ordered hierarchically porous structure. *ChemSusChem journal*. 9, 478-484.

Irie, H., Watanabe, Y., & Hashimoto, K., (2003). Synthesis and Photocatalytic study of p-type B-doped g-C_3N_4 electrode using BH_3NH_3 as the dopant precursor, *Chemistry Letters-journal*, 32, 772-773.

Jo, W.K., & Natarajan, T.S. (2015). Investigation of the influence of TiO_2 morphology on the photodegradation of isoniazid. *Chemical Engineering Journal*, 281, 549-565.

Jun, Y.S., Lee, E.Z., Wang, X.C., Hong, W.H., Stucky, G.D., & Thomas, A. (2013). Synthesis of carbon nitride hollow spheres by melamine-cyanuric acid supramolecular aggregation. *Journal of Advanced Functional Materials*, 23, 3661-3667.

Khaki, M.R.D., Shafeeyan, M.S., Raman, A.A., & Wan-Duad, M.A. (2017). Application of doped photocatalysts for organic pollutant degradation – a review. *Journal of environmental management*, 198, 78-94.

Khalid, N.R., Majida, A., Tahira, M.B., Niazb, N.A., & Khalid, S. (2017). Carbonaceous-TiO_2 nanomaterials for photocatalytic degradation of pollutants. *Ceramics international*, 43(17), 14552-14571.

Khan, S.U.M., Al-Shahry, M., & Ingler, W.B. (2002). Carbon doped titania for strong absorption to visible light. *Science*, 297, 2243-2245.

Kim, J., Lee, C.W., & Choi, W. (2010). WO_3 as an efficient photocatalyst for photoreduction of water for hydrogen production, *Journal of Environmental Science and Technolology*, 44, 6849-6854.

Kong, J.Z., Zhai, H.F., Zhang, W., Wang, S.S., Zhao, X.R., Li, M, Li, H., Li, A.D., & Wu, D. (2017). Visible Light-Driven Photocatalytic Performance of N-Doped ZnO/g-C_3N_4 Nanocomposites. *Nanoscale Research Letters*. 12, 526. DOI 10.1186/s11671-017-2297-0.

Kroke E, Schwarz M, Horath-Bordon E, Kroll P, Nollc B, & Normanc AD. (2002). Tri-s-triazine derivatives part I from trichloro-tri-s-triazine to graphitic C_3N_4 structures. *New Journal of Chemistry.* 26, 508.

Kumar, S., Surendar, T.; Baruah, A., & Shanker, V. (2013). Synthesis of a Novel and Stable g-C_3N_4-Ag_3PO_4 Hybrid Nanocomposite Photo-catalyst and Study of the Photocatalytic Activity under Visible Light Irradiation. *Journal of Materials Chemistry A*, 1, 5333−5340.

Lan, H., Li, L., An, X., Liu, F., Chen, C., Liu, H., & Qu, J. (2017). Microstructure of carbon nitride affecting synergetic photocatalytic activity. *Applied Catalysis B: Environment*. 204, 49–57. https://doi.org/10.1016/j.apcatb.2016.11.022.

Lee, K.M., Lai, C.W., Ngai, K.S., & Juan, J.C.(2016). Recent developments of zinc oxide based photocatalyst in water treatment technology: A review. *Water resources*, 88, 428-448.

Lee, Y.G., Watanabe, T., Takata, T., Hara, M., Yoshimura, M., & Domen, K. (2006). The photocatalytic activity of Ge_3N_4 for overall water splitting. *Journal of Physical Chemistry B*, 110, 17563-17569.

Li, C.H., Li, M,C., Liu, S.P., Jamison, A.C., Lee, D., Lee, T.R., & Lee, T.C. (2016a). Heteroatom doping and the profound influence on TiO_2 photocatalysis. *Journal of Applied Materials Interfaces*, 8, 9152-9161.

Li, H.Z., Zhang, X.Y., Huo, Y.N.,& Zhu, J. (2007). Synthesis of Sulfur visible-light-driven TiO_2 photocatalysts. *Journal of Environmental Science and Technology*, 41, 4410-4414.

Li, J., Shen, B., Hong, Z., Lin, B., Gao, B., & Chen, Y. A. (2013). Facile Approach to Synthesize Novel Oxygen-doped g-C_3N_4 with Superior Visible-light Photoreactivity. *Journal of Chemical Communications*, 48, 12017−12019.

Li, K., Su, F.Y., & Zhang, W.D. (2016b). Decreased quantum efficiencies as a consequence of Charge recombination during Catalysis. *Journal of Applied Surface Science*, 375, 110-117.

Li, Y.F., Li, K., Yang, Y., Li, L.J., Xing, Y., Song, S.Y., Jin, RC., & Li, M. (2015), Modification of g-C_3N_4 with oxohalides for enhanced photocatalysis, *Chemstry- European Journal*, 21, 17739-17747.

Li, Y.L., Wang, J.S., Yang, Y.L., Zhang, Y., He, D., An, Q.E., & Cao, G.Z., (2015). Synthesis various TiO_2 nanostructures and their separate doping onto g-C3N4 to create heterojunctions respectively. *Journal of Hazardous Materials*, 292, 79-89.

Li, Z., Zhan, H., Hongqi, S., Liu, S., Moses, O., Tade, S., & Wang, W. (2016c). Recent advances in non-metal modification of graphitic carbon nitride for photocatalysis: A historic review. *Jornal of Catalysis Science & Technology*, **6**(19), 7002-7023, DOI:10.1039/C6CY01195K.

Liang, Q., Li, Z., Huang, Z.H., Kang, F., & Yang, Q.H. (2015). Holey Graphitic Carbon Nitride Nanosheets with Carbon Vacancies for Highly Improved Photocatalytic Hydrogen Production. *Advanced Functional Materials.* 25(44), 6885–6892. https://doi.org/10.1002/adfm.201503221

Liang, Q.H., Li, Z., Yu, X.L., Huang, Z.H., Kang, F.Y., & Yang, Q.H. (2015b). Synthesis of macroscopic 3D porous g-C_3N_4 monolith by thermal polymerization of urea inside a unique template of melamine sponge (MS). *Journal of Advanced Material*, 27, 4634-4639.

Liao, G.Z., Chen, S., Quan, X., Yu, H.T., & Zhao, H.M., (2012). Synthesis of Graphene oxide (GO) modified g-C_3N_4 by a sonochemical approach. *Journal of Materials Chemistry*, 22, 2721 2726.

Lin, L.H., Ou, H.H., Zhang, Y.F., & Wang, X.C., (2016). Synthesis of crystalline g-C_3N_4 with tri-s-triazine subunits derived from the tri-s-triazine-based precursor for photocatalytic hydrogen production. *Journal of Catalysis*, 6, 3921-3931.

Lin, Q., Li, L., Liang, S., Liu, M., Bi, J., & Wu, L. (2015). Efficient synthesis of monolayer carbon nitride 2D nanosheet with tunable concentration and enhanced visible-light photocatalytic activities. *Journal of Applied Catalysis: B Environmental*, 163, 135–142.

Liqiang, J. (2004). Deactivation and regeneration of ZnO and TiO_2 nanoparticles in the gas phase photocatalytic oxidation of n-C_7H_{16} or SO_2. *Journal of Applied Catalysis A*, 275(1–2), 49 -54.

Liu, J., Huang, J.H., Zhou, H., & Antonietti, M. (2014). Synthesis of uniform g-C_3N_4 nanorods by a morphology-preserving route using SiO_2 nanorods as the template. *Journal of Applied Materials Interfaces*, 6, 8434-8440.

Liu, Q., Zhou,Y., Kou, J.H., Chen, X.Y., Tian, Z.P., Gao, J., Yan, S.C., & Zou, Z.G. (2010). Development of $BiWO_6$ and Zn_2GeO_4 for photocatalytic water splitting. *Journal of American Chemical Society*, 132, 14385-14387.

Liu, S.Z., Li, D.G., Sun, H.Q., Ang, H.M., Tade, M.O., & Wang, S.B., (2016). Modification of g-C_3N_4 with zinc phthalocyanine for enhanced photocalalysis. *Journal of Colloid and Interface Science*, 468, 176-182.

Liu, T.Y., & Y. Li, Y. (2016). A computational study on the effect of phosphorus doping on the electronic structure and photocatalytic performance of g-C_3N_4. *Nature Photonic journal*, 10, 361-362.

Lotsch, B.V., Doblinger, M., Sehnert,J., Seyfarth, L., Senker, J., Oeckler, O., & Schnick, W. (2007). Synthesis and Characterization of g-C_3N_4. *Chemistry-European Journal*, 13, 4969-4980.

Ma, L.T., Fan, H.Q., Wang,J., Zhao, Y.W., Tian, H.L., & Dong, G.Z. (2016). Template-free synthesis of g-C_3N_4 microspheres using a solvothermal method with melamine and cyanuric chloride as the precursors. *Journal of Applied Catalysis B-Environment*, 190, 93-102.

Ma, S.K., Hisatomi, T., Maeda, K., Moriya, Y., & Domen, K. (2012). Enhanced water oxidation on alkaline metal salts modified Ta_3N_5 photocatalyst. *Journal of American Chemical Society*, 134, 19993-19996.

Maletz, S., Foeh, T., Beier, S., Klumper, C., Brouwer, A., Benhnisch, P., Higley, E., Giesy, J.P., Hacker, M., Gebhardt, L.V., Pinnekamp, J., & Hollert, H. (2013). *In-vitro* characterization of the effectiveness of enhanced sewage processes to eliminate endocrine activity of hospital effluents. *Water Research*, 47, 1545-1557.

Mamba, G., & Mishra, A.K. (2016). Graphitic carbon nitride (g-C_3N_4) nanocomposites: a new and exciting generation of visible light driven photocatalysts for environmental pollution remediation. *Journal of Applied Catalysis B Environmental*, 198, 347–377.

Maragathavalli, S., Brindha, S., Kaviyarasi, N.S., Annadurai, B., & Gangwar, S.K. (2012). Antimicrobial activity in leaf extract of Neem (Azadirachta indica Linn). *International Journal of Science and Nature*, 3, 110-113.

Meng, Z.D., Ghosh, T., Zhu, L., Choi, J.G., Park, C.Y., & Oh, W.C. (2012). Photodegradation activity of Ag_2S on organic pollutants in water. *Journal of Materials Chemistry*, 22, 16127-16135.

Miller, T.S., Belen Jorge, A., Suter, T.M., Sella, A., Caro, F., & McMillan, P.F,. (2017). Carbon Nitrides: synthesis and characterization of a new class of functional materials. *Physical Chemistry Chemical Physics Journal*. 19. 15613-15638.

Nese,T., Sivri, N., & Toroz,I. (2007). Pollutants of textile industry wastewater and assessment of its discharge limits by water quality standards. *Turkish Journal of fisheries and Aquatic Sciences*, 7, 97-103

Niu, P., Zhang, L.L., Liu, G., & Cheng, H.M. (2012). Top-down method of thermal oxidation etching of bulk g-C_3N_4 in air, *Journal of Advanced Functional Materials*, 22, 4763- 4770.

Ong, W.J., Tan, Y.H. Ng, Y.H., Yong, S.T., & Chai, S.P. (2016). Graphitic carbon nitride (g-C_3N_4)-Based photocatalysts for artificial photosynthesis and environmental remediation. *Journal of Chemistry Review*, 116, 7159–7329.

Padmanabhan, P., Sreekumar, K., & Thiyagarajan, T. (2006). Nano-crystalline titanium dioxide formed by reactive plasma synthesis. *Vacuum Cambridge online Library*, 80 (11). 1252–1255.

Pandey, G., Verm, K.K., & Singh, M. (2014). Evaluation of phytochemical, antibacterial and free radical scavenging properties of azadirachta indica (neem) leaves. *International Journal of Pharmacy and Pharmaceutical Sciences*. 6(2), 444-447.

Pang, Y.L., Abdullah, A.Z., & Bhatia, S. (2010). Effect of annealing temperature on the characteristics, sonocatalytic activity and reusability of nanotubes TiO_2 in the degradation of Rhodamine B. *Applied catalysis B*. 100, 393-402.

Park, H., Choi, W., & Hoffmann, M.R. (2008). Synthesis of CdS hybrid photocatalysts for hydrogen production. *Journal of Materials Chemistry*, 18, 2379-2385.

Philip, D. (2010). Green synthesis of gold and silver nanoparticles using *Hibiscus rosa sinensis*, *Physica* E. 42, 1417–1424.

Pokharna, S., & Shivastava, R. (2013). Photocatalytic treatment of textile industry effluent using titanium oxide. *International Journal of Recent Research and Review*, 6(2), 9-17.

Pouretedal, H.R., Motamedi, H., & Amiri, A. (2012). Photodegradation of organic pollutants in water by ZnS. *Desalination and Water Treatement journal*, 44, 92-99.

Pradhan, G.K., Padhi, D.K., & Parida, K.M. (2013). α-Fe_2O_3 photocatalyst for water splitting and organics degradation via photocatalysis. *Journal of Applied Materials Interfaces*, 5, 9101 9110.

Rahmani, Z., Kermani, M., Gholami, A.J., & Mahmoodi, N.M., (2012). Effectiveness of photochemical and sonochemical processes in degradation of Basic Violet 16 (BV16) dye from aqueous solutions. *Iranian Journal of Environmental Health Science and Engineering*. 9, 1-7.

Ran, J.R., Ma, T.Y., Gao,G.P., Du, X.W., & Qiao, S.Z. (2015). Synthesis of porous P-doped g-C_3N_4 nanosheets by combining P doping and thermal exfoliation of a bulk material. *Journal of Energy and Environmental Science*, 8, 3708-3717.

Rehman, S., Ullah, R., Butt, A.M., & Gohar, N.D, (2009). Non metal coupling of ZnO for extending the absorption to visible light region. *Journal of Hazardous Materials*, 170, 560-569.

Rekha, K., Nirmala, M., Nair, M.G., & Anukaliani, A. (2010). Transition metal coupling of ZnO for extending the absorption to visible light region. *Physica B-Condensed Matter*, 405, 3180-3185.

Ren, W.J., Ai, Z.H., Jia, F.L., Zhang, L.Z., Fan, X.X., & Zou, Z.G. (2007). Carbon-doped TiO_2 photocatalysts prepared by different methods and their different applications. *Journal of Applied Catalysis B*, 69, 138-144.

Robinson, T., McMullan, G., Marchant, R., & Nigam, P., (2001). Remediation of dyes in textile effluent: A critical review on current treatment technologies with a proposed alternative. *International Journal of Bioresource Technology*, 77 (3). 247–255.

Rong, X.S., Qiu, F.X., Rong, J., Zhu, X.L., Yan, J., & Yang, D.Y. (2016). Synthesis of Zr-doped and W-doped g-C_3N_4 for enhanced photocatalysis. *Materials Letters-journal*, 164, 127-131.

Sadi, S.A., Devi, G.M., Syed, M.A., Feroz, S., & Varghese, M.J. (2015). Treatment of textile industry wastewater using solar photocatalysis. *Research journal of chemical science*, 5(10), 20-27.

Sakthivel, S., Shankar, M.V., Palanichamy, M., Arabindoo, B., Bahnemann, W., & Murugesan, V. (2004). Enhanced TiO_2 photocatalysis. *Journal of Water Resources*, 38, 3001-3008.

Sang, Y.H., Zhao, Z.H., Zhao, M.W., Hao, P., Leng, Y.H., & Liu, H. (2015). Photodegradation activity of WS_2 on organic pollutants in water. *Journal of Advanced Materials*, 27, 363- 369.

Sarnali, M., & Bhagchandani, C.G. (2016). Novel wastewater treatment technique in textile industry. *International journal of advanced research and innovative ideas in education*, 2(3), 2435-2349.

Satyawali, Y., & Balakrishnan, M., (2008). Wastewater treatment in molasses-based alcohol distilleries for COD and color removal: A review. *Journal of Environmental Managemen*t, 86 (3), 481–497

Seredych, M., Los, S., Giannakoudakis, D.A., Rodriguez-Castellon, E., & Bandosz, T.J. (2016). Synthesis of g-C_3N_4/S-doped porous carbon composite and its photoactivity. *ChemSusChem - Journal*, 9, 795-799.

Shalom, M., Inal, S., Fettkenhauer, C., Neher, D., & Antonietti, M. (2013). Synthesis of ordered, hollow carbon nitride structure using a cyanuric acid-melamine complex as the precursor. *Journal of American Chemical Society*, 135, 7118-7121.

She, X.J., Liu, L., Ji, H.Y., Mo, Z., Li, Y.P., Huang, L.Y., Du, D.L., Xu, H., & Li, H.M. (2016). Template-free synthesis of 2D porous ultrathin g-C_3N_4 nanosheets. *Journal of Applied Catalysis B-Environment*, 187, 144-153.

Shi, H.F., Chen, G.Q., Zhang, C.L., & Zou, Z.G. (2014). Modification of g-C_3N_4 with $NaNbO_3$ for enhanced photocatalysis. *American Chemical Society-Catalysis*, 4, 3637-3643.

Shi, L., Liang, L., Wang, F., Liu, M., Zhong, S., & Sun, J. (2015). Tetraethylorthosilicate induced Preparation of mesoporous graphitic carbon nitride with improved visible light Photocatalytic activity. *Journal of Catalysis Communications*, 59, 131–135.

Sokolovskii, V. D. (1990). Principles of Oxidative Catalysis on Solid Oxides. *Journal of Catalysis Review*, 32, 1−49.

Spanhel, L., Weller, H., & Henglein, A. (1997). Doping of TiO_2 for surface modification and sensitization. *Journal of American Chemical Society*, 109, 6632-6635.

Stolbov, S., & Zuluaga, S. (2013). First-principles study on the effect of sulfur doping on the electronic and geometric structures of g-C_3N_4. *Journal of Physics-Condensed Matter*, 25, 5154-5159.

Subapriya R, & Nagini S. (2005). Medicinal properties of neem leaves: a review. *Current Medicinal Chemistry*: Anticancer Agents. 5,149-160.

Sun, H., Ang, H.M., Tade, M.O., & Wang, S. (2013). Metal-based catalysis involving metal oxides. *Journal of Materials Chemistry A*, 1, 14427-14442.

Sun, H.Q., Bai, Y., Jin, W.Q., & Xu, N.P. (2008). Photocatalysis of N-TiO_2 sysytem. *Journal of Solar Energy Materrials*, 92, 76-83.

Sun, H.Q., Feng, X.H., Wang, S.B., Ang, H.M., & Tade, M.O. (2011). The applications of doped TiO_2 or other metal oxide photocatalysts. *Chemical Engineering Journal*, 170, 270-277.

Sun, H.Q., Liu, S.Z., Liu, S.M., & Wang, S.B. (2014). efficient photocatalytic activityof ZO_2. *Journal of Applied Catalysis B-Environ*, 146, 162-168.

Sun, H.Q., Wang, S.B., Ang, H.M., Tade, M.O., & Li, Q. (2010). Synthesis of halogen elements visible-light-driven TiO_2 photocatalysts. *Chemical Engineering Journal*, 162, 437-447.

Sun, H.Q., Zhou, G.L., Wang, X.Y., Suvorova, A., & Wang, S.B. (2014). Toxic metal leaching from photo-corrosion as significant barriers of metal-based photocatalysts to practical applications. *Journal of Applied Materials Interfaces*, 6, 16745-16754.

Tachibana, Y., Vayssieres, L., & Durrant, J.R. (2012). Artificial photosynthesis for solar water splittin. *Journal of Nature Photonics* 6, 511–518.

Takanabe, K., Kamata, K., Wang, X.C., Antonietti, M., Kubota, J., & Domen, K. (2010). The application of Magnesium phthalocyanine (MgPc) dye sensitization of mesoporous carbon nitride for highly efficient hydrogen evolution. *Physical Chemistry Chemical Physics- Journal*, 12, 13020-13025.

Thomas, A., Fischer, A., Goettmann, F., Antonietti, M., Muller, J.O., Schlogl, R., & Carlsson, J. M. (2008). Graphitic Carbon Nitride Materials: Variation of Structure and Morphology and Their Use as Metal-Free Catalysts. *Journal of Materials Chemistry*, 18, 4893−4908.

Tian, Y., & Tatsuma, T. (2005). Plasmon-induced photo-electrochemistry in the visible light region on Au-TiO_2 composite. *Journal of American Chimerical Society*, 127, 7632-7637.

Tonda, S., Kumar, S., Kandula, S., & Shanker, V. (2014). Fe-doped and mediated graphitic carbon nitride nanosheets for enhanced photocatalytic performance under natural sunlight. *Journal of Materials Chemistry: A*, 2, 6772.

Tsugi, I., Shimodaira, Y., Kato, H., Kobayashi, H., & Kudo, A. (2010). Photodegradation activity of A_2(I)-Zn-A(IV)-S_4 (A(I) = Cu and Ag; A(IV) = Sn and Ge) on organic pollutants in water. *Chemical Materials journal*, 22, 1402-1409

Uddin, M.T., Nicolas, Y., Olivier, C., Toupance, T., Servant, L., Muller, M.M.., Kleebe, H.J., Ziegler, J., & Jaegermann, W. (2012). Semiconductor coupling of ZnO for extending the absorption to visible light region. *Journal of Inorganic Chemistry*, 51, 7764-7773.

Vani, P., Manikandan, N., & Vinitha, G. (2017). A green strategy to synthesize environmentally friendly metal oxide nanoparticles for potential applications. *Asian journal of pharmaceutical and clinical research*. Special issue, 337-343.

Verma, A., & Mehata, M.S. (2016). Controllable synthesis of silver nanoparticles using Neem leaves and their antimicrobial activity. *Journal of Radiation Research and Applied Sciences.* 9(1), 109-115.

Wang, F., Ng, W.K.H., Yu, J.C., Zhu, H.J., Li, HC.H., Zhang, L., Liu, Z.F., & Li, Q. (2012a). The modification methods for varying the band structures of g-C_3N_4 by doping and copolymerization. *Journal of Applied Catalysis B-Environment*, 111, 409-414.

Wang, H., Fang, L., Hu, S., Pei, Y., & Ma, W. (2018). A green and facile method to prepare graphitic carbon nitride nanosheets with outstanding photocatalytic H_2O_2 production ability via NaClO hydrothermal treatment. *New journal of chemistry*. 42, 18335- 18341.

Wang, J.H., Zhang, C., Shen, Y.F., Zhou, Z.X., Yu, J.C., Li, Y., Wei, W., Liu, S.Q., & Zhang, Y.J. (2015). Synthesis of porous g-C_3N_4 using calcium carbonate as a template. *Journal of Materials Chemistry*, A, 3, 5126-5131.

Wang, X., Blechert, S., & Antonietti, M. (2012). Polymeric Graphitic Carbon Nitride for Heterogeneous Photocatalysis. *American Chemical Society*, 2, 1596−1606.

Wang, X., Maeda, K., Chen, X., Takanabe, K., Domen, K., Hou, Y., Fu, X., & Antonietti, M. (2009). Polymer Semiconductors for Artificial Photosynthesis: Hydrogen Evolution by Mesoporous Graphitic Carbon Nitride with Visible Light. *Journal of American Chememical Society*, 131, 1680−1681.

Wang, Y,J., Shi, R., Lin, J., & Zhu, Y.F. (2011). Synthesis of ZnO hybridized g-C_3N_4 by a monolayer-dispersed method. *Journal of Energy Environmental Science*, 4, 2922-2929.

Wang, Y., Di, Y., MAntonietti, M., Li, H.R., Chen, X.F., & Wang, X.C. (2010). Photocatalytic activity of Fluorinated g-C_3N_4 prepared by directly incorporating NH_4F into the thermal condensation process in g-C_3N_4 synthesis. *Chemistry of Materials- journal*, 22, 5119- 5121.

Wang, Y., Wang, X.C., & Antonietti, M. (2012). Application of Carbon nitride in various catalytic reactions. *Angewandte Chemie International Edition*, 51, 68-89.

Wang, Y.B., Hong, J.D., Zhang, W., & Xu, R. (2013). Dye sensitization of carbon nitride nanosheets Erthrosin B (ErB). *Journal of Catalysis Science and Technology*, 3, 1703-1711.

Wu, L., Yu, J.C.,& Fu, X.Z., (2006). Modification of TiO_2 with metal sulfides such as CdS, MoS_2 and WS_2, for efficient responce to visible ligh. *Journal of Molecular Catalysis A*, 244, 25-32.

Wu, W.T., Zhang, J.Q., Fan, W.Y., Li, Z.T., Wang, L.Z., Li, X.M., Wang, Y., Wang, R.Q., Zheng, J.T., Wu, M.B., & Zeng, H.B. (2016). The use of melamine to remedy various defects of mesoporous g-C_3N_4 for photo-oxidation reactions of 1,4-dihydro-2,6-dimethylpyridine-3,5-dicarboxylate (1,4-DHP). *Amerian Chemical Society-Catalysis*, 6, 3365-3371.

Xiang, Q.J., Yu, J.G., & Jaroniec, M. (2011). Heteroatom doping: co-doping with nitrogen by non metals for photocatalysis. *Journal of Physical Chemistry*, 13, 4853-4861.

Xu, A.W., Gao, Y, & Liu, H.Q. (2002). Introducing transition metal ions as dopants for TiO_2. *American Chemical Society*, 133, 2362−2365.

Xu, J.Y., Li, Y.X., Peng, S.Q., Lu, G.S., & Li, S.B. (2013). Dye sensitization of carbon nitride using Eosin Y (EY) for quantum yield in hydrogen evolution. *Physical Chemistry Chemical Physics- Journal*, 15, 7657-7665.

Xu, X., Zheng, Z., Zhang, L.Z., Zhang, H.L., & Deng, F. (2008). Cu_2O as an efficient photocatalytic splitting of water for hydrogen production. *Journal of Solid State Chemistry*, 81, 2516-2522.

Yan, H.J., & Yang, H.X. (2011). Coupling TiO_2 to C_3N_4 as a modification route for increased photocatalytic hydrogen evolution rate efficiency. *Journal of Alloys and Compounds*, 509, L26-L29.

Yan, S.C., Li, Z.S., & Zou, Z.G. (2010). Synthesis of Boron-doped g-C_3N_4 by heating a mixture of melamine and boron oxide and its photocatalytic efficiency on Rhodamine B (Rh B) degradation. *Langmuir-journal*, 26, 3894-3901.

Yang, H., & Cheng, H., (2007). Controlling nitrite level in drinking water by chlorination and chloramination. *Journal of Separation and Purification Technology*, 56 (3). 392–396.

Yang, S., Gong, Y., Zhang, J., Zhan, L., Ma, L., Fang, Z., Vajtai, R., Wang, X., & Ajayan, P.M. (2013). Exfoliated graphitic carbon nitride nanosheets as efficient catalysts for hydrogen evolution under visible light, *Journal of Advanced Materials*. 25, 2452–2456.

Yang, X.L., Qian, F.F., Zou, G.J., Li, M.L., Lu, J.R., Li, Y.M., & Bao, M.T. (2016). Properties and applications of g-C_3N_4. *Journal of Applied Catalysis B-Environental*, 193, 22-35.

Yang, Z., Zhang, Y.J., & Schnepp, Z. (2015). Structural modification of g-C_3N_4 using soft, hard templates and biotemplates. *Journal of Materials Chemistry A*, 3, 14081-14092.

Yao, Y.J., Lu, F., Zhu, Y.P., Wei, F.Y., Liu, X.T., Lian, C., & Wang, S.B. (2015). Modification of g-C_3N_4 with $CuFe_2O_4$ for enhanced photocatalysis. *Journal of Hazardous Materials*, 297, 224-233.

YashRoy, R.C., & Gupta, P.K. (2000). Neem-seed oil inhibits growth of termite surface-tunnels. *Indian Journal of Toxicology*, 7 (1), 49–50.

Ying, T. (2015). Application of TiO particles on wastewater treatment. MSc. Thesis, Perkin University, National University of Singapore, 35-40.

Yozana, N., (2015). Green synthesis of nano-structured TiO_2 using Aspalathus Linearis Extract. B-tech Chemistry thesis, Department of Chemistry, University of Western Cape.38-74.

Yu, Z., Yin, B.S., Qu, F.Y., & Wu, X. (2014). Synthesis of modified CdS for photodegradation of organic pollutants in water. *Chemical Engineering Journal*, 258, 203-209.

Zaleska, A., Sobczak, J.W., Grabowska, E., & Hupka, J. (2008). Synthesis of Boron visible-light-driven TiO_2 photocatalysts. *Journal of Applied Catalysis B-Environmental*, 78, 92-100.

Zhang, J., Sun, J., Maeda, K., Domen, K., Liu, P., Antonietti, M., Fu, X., & Wang, X. (2011). Sulfur-mediated Synthesis of Carbon Nitride: Band-gap Engineering and Improved Functions for Photocatalysis. *Journal of Energy and Environtal Science*, 4, 675−678.

Zhang, J.S., Chen, Y., & Wang, X.C. (2015). Synthesis methods of g-C_3N_4 nanosheets. *Journal of Energy and Environmental Science*, 8, 3092-3108.

Zhang, J.S., Sun, J.H., Maeda, K., Domen, K., P. Liu, P., Antonietti, M., Fu, X.Z., & Wang, X.C. (2011). Development of sulfur-mediated synthesis to stimulate carbon nitride bulk condensation by trithiocyanuric as the precursor. *Journal of Energy and Environmental Science*, 4, 675-678.

Zhang, J.S., Zhang, G.G., Chen, X.F., Lin, S., Mohlmann, L., Dolega, G., Lipner, G., Antonietti, M., Blechert, S., & Wang, X.C. (2012). The use of various monomer building blocks with desired compositions and electronic structures for modification of g-C_3N_4. *Angewandte Chemie International Edition*, 51, 3183-3187.

Zhang, L.L., Xiong, Z.G., & Zhao, X.S. (2010). Synthesis of Phosphorus-doped g-C_3N_4 by poly-condensation of the precursor of g-C_3N_4 (dicyandiamide) and a phosphorus-containing ionic liquid heteroatom source. *ACS Nano journal*, 4, 7030-7036.

Zhang, L.W., Cheng, H.Y., Zong, R.Z., & Zhu, Y.F. (2009). Poor stability of ZnO as a consequence of photo-corrosion. *Journal of Physical Chemistry C*, 113, 2368-2374.

Zhang, M., Luo, W., Wei, Z., Jiang, W., Liu, D., & Zhu, Y.(2016). Synthesis of 3D C_3N_4-agar hydrogel photocatalyst and C_3N_4/SiO_2 hydrogels and their photocatalytic activities. *Journal of Applied Catalysis B: Environment*, 194, 105-110.

Zhang, M., Xu, J., Zong, R., & Zhu, Y. (2014). Enhancement of Visible Light Photocatalytic Activities via Porous Structure of g-C_3N_4. *Journal of Applied Catalysis B*, 147, 229−235.

Zhang, Y., Liu, J., Wu, G., & Chen, W. (2012). Porous graphitic carbon nitride synthesized via direct polymerization of urea for efficient sunlight-driven photocatalytic hydrogen production. *Nanoscale*, 4, 5300−5303.

Zhang, Y.J., Schnepp, Z., Cao, J.Y., Ouyang, S.X., Li, Y., Ye, J. H., & Liu, S.Q. (2013). Synthesis of a sponge-like structure of graphitic carbon nitride via biopolymer-activation through soft-templating using seaweed polysaccharide or gelatin. *Scientific Reports journal*, 3, ARTN 2163.

Zhang, Z.Y., Jiang, D.L., Li, D., He, M.Q., & Chen, M. (2016). Modification of g-C_3N_4 with $SnNb_2O_6$ nanosheet for enhanced photocatalysis. *Journal of Applied Catalysis B-Environment*, 183, 113-123.

Zhao, H., Dong, Y., Jiang, P., Miao, H., Wang, G., & Zhang, J. (2015). In situ light-assisted preparation of MoS_2 on graphitic C_3N_4 nanosheets for enhanced photocatalytic H_2 production from water. *Nanoscale Journal*, 7, 15-37.

Zhao, Z.K., Dai, Y.T., Lin, J.H., & Wang, G.R. (2014). Synthesis of mesoporous carbon nitride nanorods using SBA-15 as the template and hexamethylenetetramine as the precursor. *Chemistry of Materials journal*, 26, 3151-3161.

Zheng, Y., Lin, L.H., Wang, B., & Wang, X.C. (2015). Synthesis and modification of tailored g-C_3N_4 photocatalysts for water splitting. Angewandte Chemie International Edition, 53, 12868-12884.

Zheng, Y., Lin, L.H., Ye, X.J., Guo, F.S., & Wang, X.C. (2014). Synthesis of helical g-C_3N_4 with a twisted hexagonal rod-like morphology via nanocasting with chiral SiO_2 templates. *Angewandte Chemie International Edition*, 53, 11926-11930.

Zheng, Y., Liu, J., Liang, J., Jaroniec, M., & Qiao, S.Z. (2012). The synthesis of g-C_3N_4 with controllable structures and morphologies. *Journal of Energy and Environmental Science*, 5, 6717-6731.

Zhou, L., Wang, W.Z., Xu, H.L., Sun, S.M., & Shang, M. (2009). Splitting of water for hydrogen production by Bi_2O_3 photocatalyst. *Chemistry-European Journal*, 15, 1776-1782.

Zhou, Y.J., Zhang, L.X., Huang, W.M., Kong, Q.L., Fan, X.Q., Wang, M., & Shi, J.L. (2016). Synthesis of N-doped g-C_3N_4 using citric acid and urea as the starting precursors for the thermal polymerization. *Carbon*, 99, 111-117.

Zhu, J. J., Faria, J. L., Figueiredo, J. L., & Thomas, A. (2011). ReactionMechanism of Aerobic Oxidation of Alcohols Conducted onActivated-Carbon-Supported Cobalt Oxide Catalysts. *European Journal of Chemistry*, 17, 7112−7117.

Zhu, J. J., Yang, X. G., Xu, X. L., Wei, K. M. (2007). Active Site Structure of NO Decomposition on Perovskite(-Like) Oxides: An Investigation from Experiment and Density Functional Theory. *Journal of Physical Chemistry* C, 111, 1487−1490.

Zhu, J. J.; Thomas, A. (2009). Perovskite-Type Mixed Oxides as Catalytic Material for NO Removal. *Journal of Applied Catalysis B*, 92, 225−233.

Zhu, J., Wang, T., Xu, X., Xiao, P., Li, J. (2013). Pt Nanoparticles Supported on SBA-15: Synthesis, Characterization and Applications in Heterogeneous Catalysis. *Journal of Applied Catalysis B*, 131, 197−217.

Zhu, J., Xiao, P., Li, H., Carabineiro, S.A.C. (2014). Graphitic Carbon Nitride: Synthesis, Properties, and Applications in Catalysis. *Journal of applied and materials interfases*. 6, 16449−16465.

Zhu, T.T., Song, Y.H., Ji, H.Y., Xu, Y.G., Song, Y.X., Xia, J.X., Yin, S., Li, Y.P., Xu, H., Zhang, Q., Li, H.M. (2015). Synthesis of template free mesoporous P-doped g-C_3N_4 nanostructured flowers by co-condensation method. *Chemical Engineering Journal*, 271, 96-105.

Zhu, Y., Zaera, F. (2014). Selectivity in the Catalytic Hydrogenation of Cinnamaldehyde Promoted by Pt/SiO_2 as a Function of Metal Nanoparticle Size. *Catalysis Science and Technology*. 4, 955−962.

Zong, X., Wu, G.P., Yan, H.J., Ma, G.J., Shi, J.Y., Wen, F.Y., Wang, L., Li, C. (2010). Synthesis of CdS for hydrogen production from water under visible light photocatalysis. *Journal of Physical Chemistry C*, 114, 1963-1968.

Zou, J.P., Wang, L.C., Luo, J.M., Nie, Y.C., Xing, Q.J., Luo, X.B., Du, H.M., Luo, S.L., Suib, S.L. (2016). Synthesis of g-C_3N_4 hybrid photocatalyst using Graphene quantum dots. *Journal of Applied Catalysis B-Environment*, 193, 103-109.

APPENDIX A

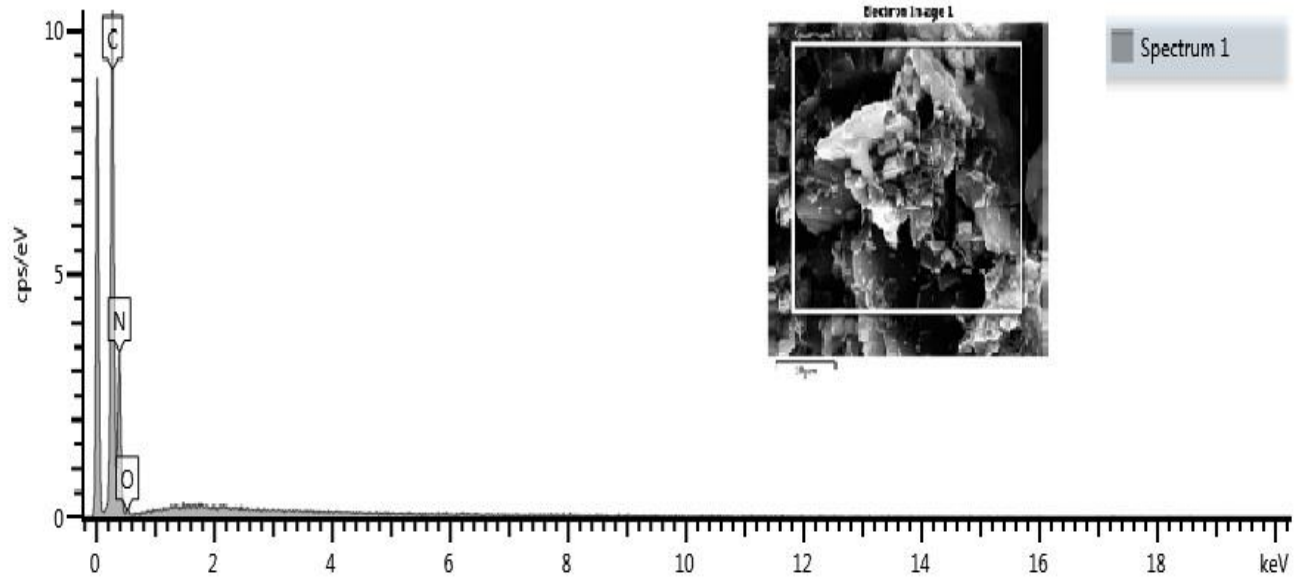

EDS Spectra of Modified g-C_3N_4

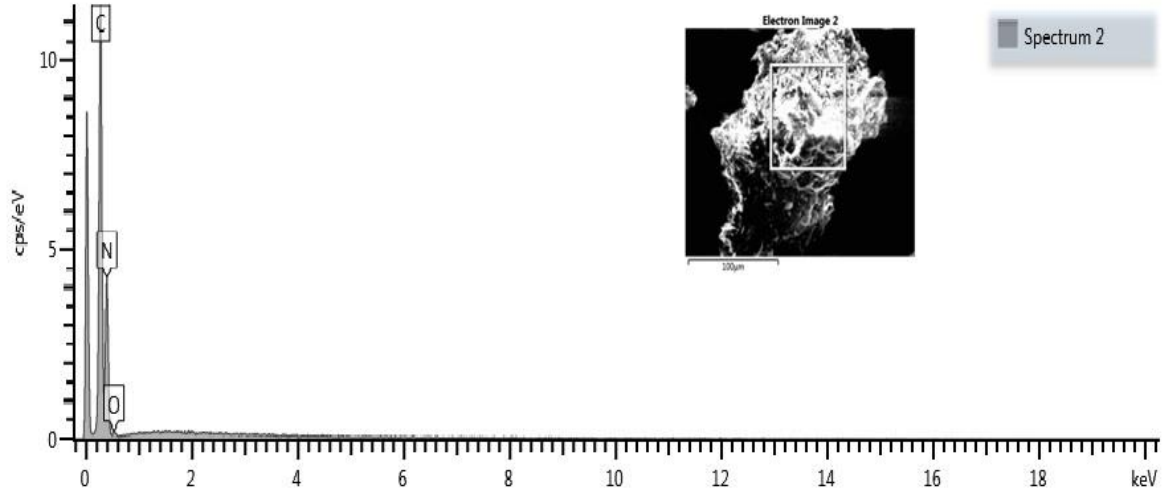

EDS Spectra of Unmodified g-C_3N_4

APPENDIX B

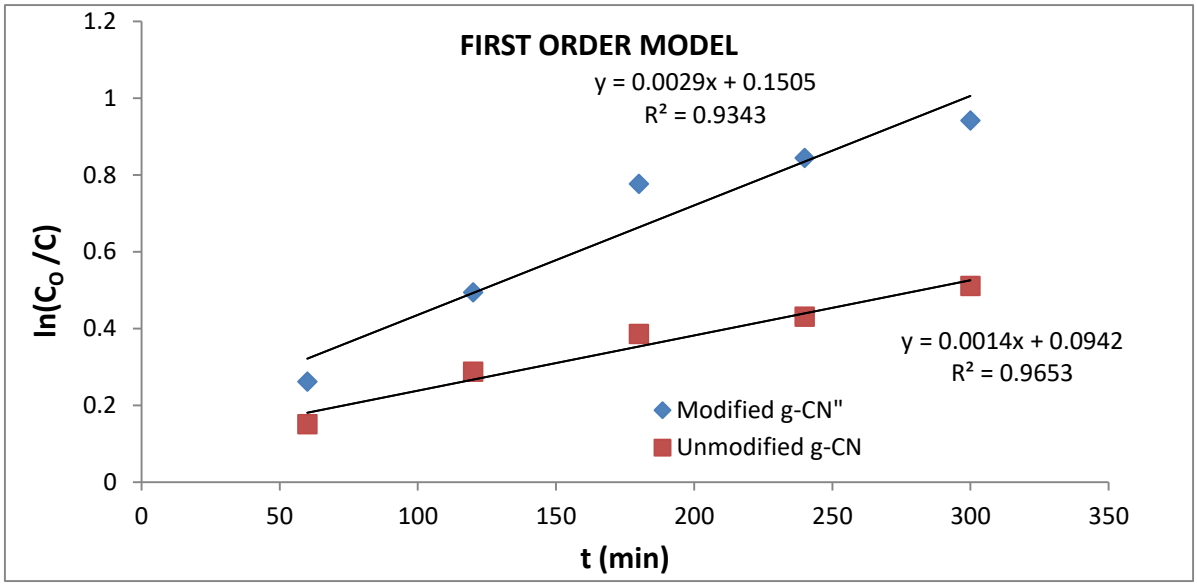

First Oder plot of the reduction of COD in the local dyeing wastewater by g-C_3N_3 nanoparticles

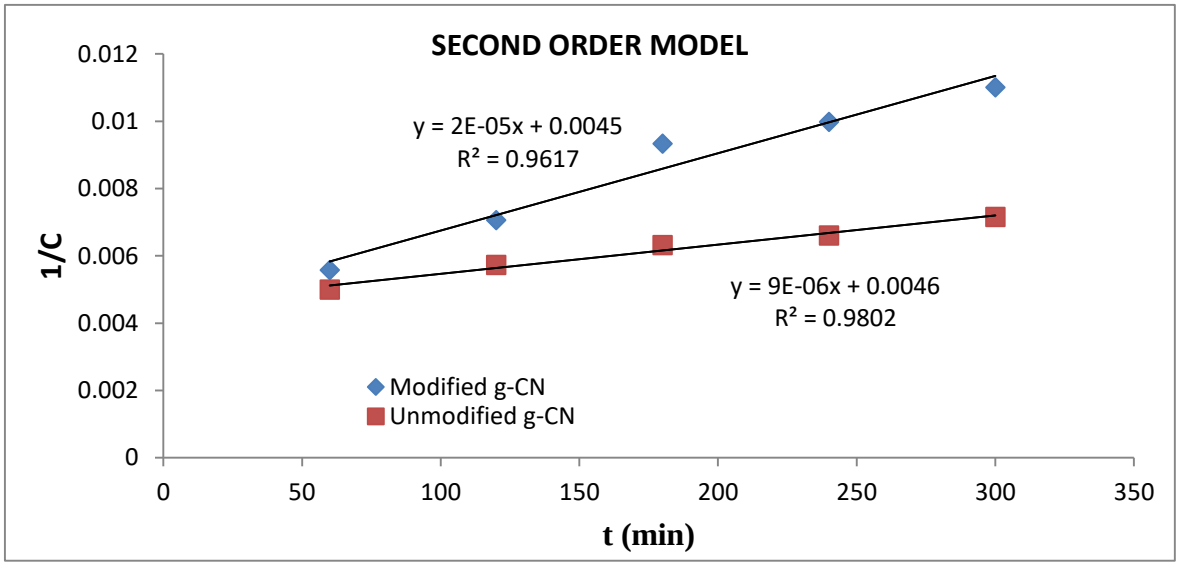

Second order plot

APPENDIX C

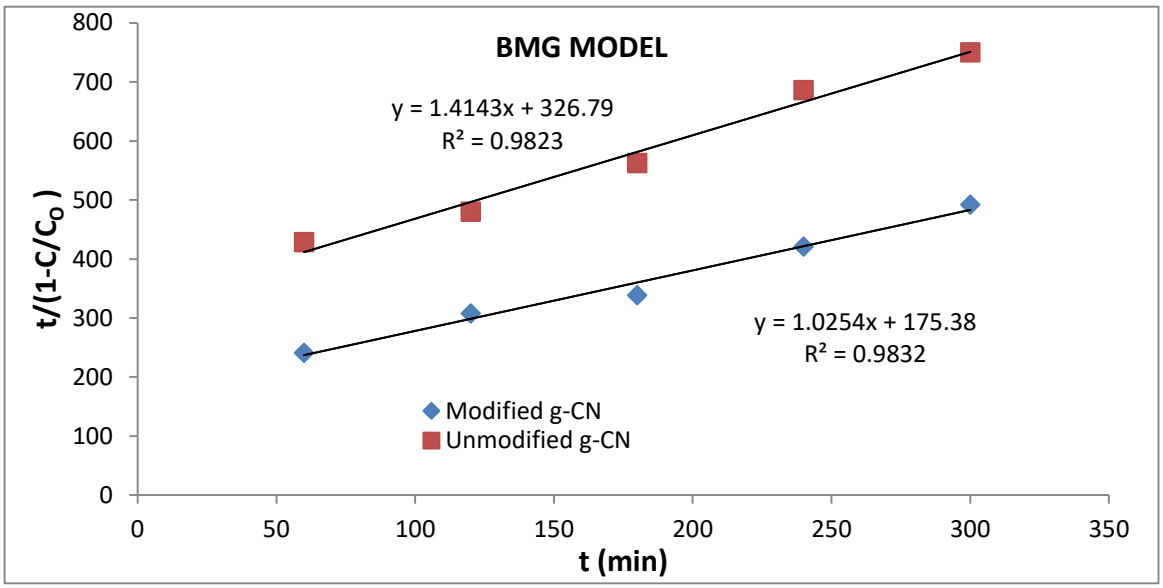

Behnjady- Modirshahla- Ghanbery (BMG) plot